



# Performance of Biogas-Fed Solid Oxide Fuel Cells

A Major Qualifying Project Report submitted to the Faculty of

WORCESTER POLYTECHNIC INSTITUTE

Chemical Engineering Department

in partial fulfillment of the requirements for the Degree of Bachelor of Science

Submitted by:

---

Courtney Jones

April 28, 2016

Advisor: Ravindra Datta

Co-Advisor: Joshua Persky (Protonex)

This report represents the work of WPI undergraduate students submitted to the faculty as evidence of completion of a degree requirement. WPI routinely publishes these reports on its website without editorial or peer review. For more information about the projects program at WPI, please see <http://www.wpi.edu/academics/ugradstudies/project-learning.html>

## Abstract

Biogas, a renewable fuel produced from organic waste, is commonly used for cooking and heating in rural or developing communities. The focus of this study was to investigate the use of this biogas (50-70% CH<sub>4</sub> and 20-50% CO<sub>2</sub>) in a solid oxide fuel cell (SOFC) to produce electricity. Research in literature has been done on biogas use with button (differential) cells, but no research has been performed with larger-scale tubular cells, a geometry more indicative of performance of a larger practical unit. Both humidified and dry biogas compositions were tested and the cell's outlet gas composition was analyzed with a mass spectrometer. Stable single-cell operation was achieved for 250 hours at 12 watts under humidified biogas at 900°C with minimal degradation. Single cell polarization and durability results were obtained for different feed gas compositions. Finally, a 5-cell SOFC assembly was tested to simulate a larger practical unit. A small school in Chhattisgarh, India uses about 465 kWh of electricity per year. One 25-cell biogas-SOFC stack has the ability to be a primary power source for the school (~2,000 kWh), or be integrated into a solar-SOFC-battery hybrid system.

## Acknowledgements

I would like to first thank my advisors, Ravindra Datta and Joshua Persky, for their guidance and support with this project. In addition, thank you to Protonex for providing me with endless resources, from employees' insights and skills to advanced equipment, that made this project successful. Thank you to WPI's chemical engineering department for managing the important administrative work involved in MQP projects and presentations. Lastly, thank you to WPI for the opportunity to take part in exciting and meaningful research. The knowledge and skills that I have gained will be carried with me in all of my future endeavors.

## Table of Contents

|  |    |
|--|----|
| Abstract.....  | 2  |
| Acknowledgements.....  | 3  |
| Table of Contents.....   | 4  |
| Table of Figures.....  | 5  |
| 1. Introduction.....   | 6  |
| 2. Literature Review.....  | 11 |
| 2.1 Fuel Cells as an Energy-Producing Technology.....  | 11 |
| 2.2 Harnessing Biogas.....   | 26 |
| 2.3 Pairing Biogas with SOFCs.....   | 30 |
| 3. Methodology.....  | 39 |
| 3.1 Effect of Biogas Composition on SOFC Performance.....                                      | 41 |
| 3.2 Effect of Fuel Utilization on SOFC Lifetime.....   | 43 |
| 3.3 Effect of Moisture in Feed on Cell Lifetime.....   | 50 |
| 3.4 Mass Spectrometry Analysis on the Outlet Gas of the Single-Cell SOFC.....                  | 50 |
| 3.4 Effects of 45:55 CH <sub>4</sub> :CO <sub>2</sub> Fuel Through a 5-Cell SOFC Assembly..... | 53 |
| 4. Results and Discussion.....   | 55 |
| 4.1 Effect of Biogas Composition on SOFC Performance.....                                      | 55 |
| 4.2 Effect of Fuel Utilization on SOFC Lifetime.....   | 61 |
| 4.3 Effect of Moisture in Feed on Cell Lifetime.....   | 63 |
| 4.4 Mass Spectrometry Analysis on the Outlet Gas of the Single-Cell SOFC.....                  | 65 |
| 4.5 Effects of 45:55 CH <sub>4</sub> :CO <sub>2</sub> Fuel Through a 5-Cell SOFC Assembly..... | 68 |
| 5. Conclusions and Commercialization Potential.....  | 70 |
| 5.1 Conclusions.....   | 70 |
| 5.2 Commercialization Potential.....   | 70 |
| 5.3 Recommendations for Future Work.....   | 72 |
| References.....  | 74 |
| Appendices.....  | 78 |
| Appendix A.....  | 78 |
| Appendix B.....  | 79 |
| Appendix C.....  | 84 |

## Table of Figures

|   |    |
|---|----|
| Figure 1: a) Biodigester diagram (Services, 2012), b) Constructed biodigester (The Biodigester, 2014).                                      | 6  |
| Figure 2: Biodigester-SOFC system flow chart.   | 7  |
| Figure 3: Typical tubular solid oxide fuel cells (Tubular, n.d.).   | 8  |
| Figure 4: Fuel cell market size projection (Fuel Cell Technology, 2014).  | 12 |
| Figure 5: Operation of PEMFC or PAFC (Technologies, 2016).  | 14 |
| Figure 6: Operation of AFC (Technologies, 2016).  | 16 |
| Figure 7: Operation of MCFC (Technologies, 2016).   | 17 |
| Figure 8: Operation of SOFC (Technologies, 2016).   | 18 |
| Figure 9: Plot of low temperature polarization curve with overpotentials (Introduction, 2012).  | 20 |
| Figure 10: Polarization plot for pure hydrogen and CO with power density (Homel et al., 2010).  | 26 |
| Figure 11: Biodigester to cooking stove process (Taherzadeh, 2012).   | 27 |
| Figure 12: Biochemical process of anaerobic digestion (Anaerobic, n.d.).  | 28 |
| Figure 13: Effect of temperature on methane production (Vindis and Mursec, 2009).   | 29 |
| Figure 14: Temperature effect on biogas conversion (Lanzini et al., 2013).  | 31 |
| Figure 15: Temperature effect on carbon deposition (Lanzini et al., 2013).  | 32 |
| Figure 16: Current required to suppress various amounts of carbon formation (Mermelstein et al., 2011).                                     | 35 |
| Figure 17: 800 hour button cell test (Shiratori et al., 2010).  | 36 |
| Figure 18: a) 500 hour test for 60 mm <sup>3</sup> button cell, b) 500 hour test for 80 mm <sup>3</sup> button cell (Papadam et al., 2012). | 37 |
| Figure 19: Bloom Energy Server <sup>®</sup> at Apple's data center (Fehrenbacher, 2013).  | 38 |
| Figure 20: PFD for the biogas-SOFC system.  | 39 |
| Figure 21: T-SOFC Test Stand Set-Up.  | 40 |
| Figure 22: mks Spectra Products Mass Spectrometer.  | 41 |
| Figure 23: Universal Data Acquisition (UDA) Software Interface.   | 43 |
| Figure 24: Gibbs free energy for the DR and RWGS reactions.   | 45 |
| Figure 25: MS capillary in the outlet end of the fuel cell.   | 51 |
| Figure 26: H <sub>2</sub> and CO MS calibration curve.  | 52 |
| Figure 27: 5-Cell T-SOFC Assembly.  | 53 |
| Figure 28: Polarization curves for 5 CH <sub>4</sub> :CO <sub>2</sub> ratios and pure H <sub>2</sub> and CO.                                | 56 |
| Figure 29: OCV Values for various CH <sub>4</sub> :CO <sub>2</sub> ratios.  | 57 |
| Figure 30: Lifetime plot for 60:40 CH <sub>4</sub> :CO <sub>2</sub> at 700°C and 0.7 V.   | 58 |
| Figure 31: Lifetime plots for 4 CH <sub>4</sub> :CO <sub>2</sub> ratios.  | 59 |
| Figure 32: Lifetime plots for five different fuel utilizations.   | 62 |
| Figure 33: Polarization curve for before and after 250 hours of operation at 76% fuel utilization.  | 63 |
| Figure 34: Degradation rates for cells running with and without water at different utilizations.  | 64 |
| Figure 35: Change in composition of species for incremental current values.   | 66 |
| Figure 36: H <sub>2</sub> and CO composition and respective and total power generation for incremental current values.                      | 68 |
| Figure 37: Polarization curve for 5-cell stack on biogas.   | 69 |

## 1. Introduction

Methane ( $\text{CH}_4$ ) and carbon dioxide ( $\text{CO}_2$ ) are two greenhouse gases that are emitted through anaerobic fermentation of organic waste. This gas mixture is commonly called biogas and consists of 50-75%  $\text{CH}_4$ , 25-50%  $\text{CO}_2$ , and trace amounts of water ( $\text{H}_2\text{O}$ ), nitrogen ( $\text{N}_2$ ), hydrogen ( $\text{H}_2$ ), and hydrogen sulfide ( $\text{H}_2\text{S}$ ) (*Biogas*, n.d.). About 30% of the U.S.'s  $\text{CH}_4$  emissions in 2013 originated from the biogas produced at landfills and livestock sites (EPA, n.d.). To prevent these emissions, a common method of harnessing the biogas is with a biodigester. Biodigesters can be found in rural communities and developing areas of countries where centralized electricity is impractical or unavailable. Figure 1a shows a diagram of a typical biodigester, and Figure 1b shows a biodigester that has been implemented in Cambodia.

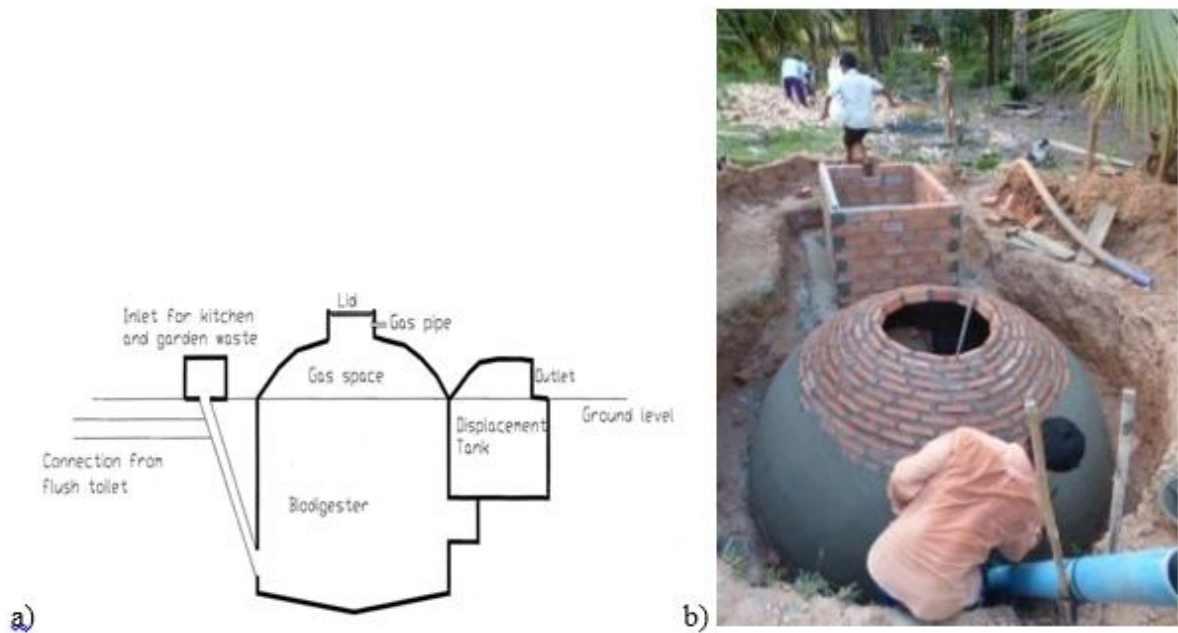


**Figure 1:** a) *Biodigester diagram* (Services, 2012), b) *Constructed biodigester* (The Biodigester, 2014).

In the 1970s the Chinese government “promoted biogas use in every rural family” and facilitated the installation of over 7 million biodigesters. These areas, however, primarily use the biogas for cooking stoves. When biogas is combusted, it produces  $\text{CO}$  and  $\text{CO}_2$ , leading to high levels of air

pollution (Bond and Templeton, 2011). These areas could greatly benefit from access to affordable and reliable technology that allows biogas to directly produce electricity. This study investigates the use of biogas in a solid-oxide fuel cell (SOFC) to produce electricity.

Fuel cell technology converts chemical energy stored in a fuel to electrical energy to produce electricity. Most types of fuel cells operate on either  $H_2$  or externally reformed fuels to obtain good performance and to prevent damaging the cell (Fuel Cell Energy, n.d.). However, pure hydrogen is impractical due to its high cost and difficulty with storage and transportation, and externally reforming fuels is costly, complex, bulky, and inefficient. Solid oxide fuel cells (SOFC) relieve these difficulties with their high operating temperature (700 – 1,000 °C) and thus, ability to internally reform hydrocarbons and to simultaneously produce utilizable heat (Protonex, n.d.). Figure 2 shows a flow diagram of a biodigester-SOFC system.

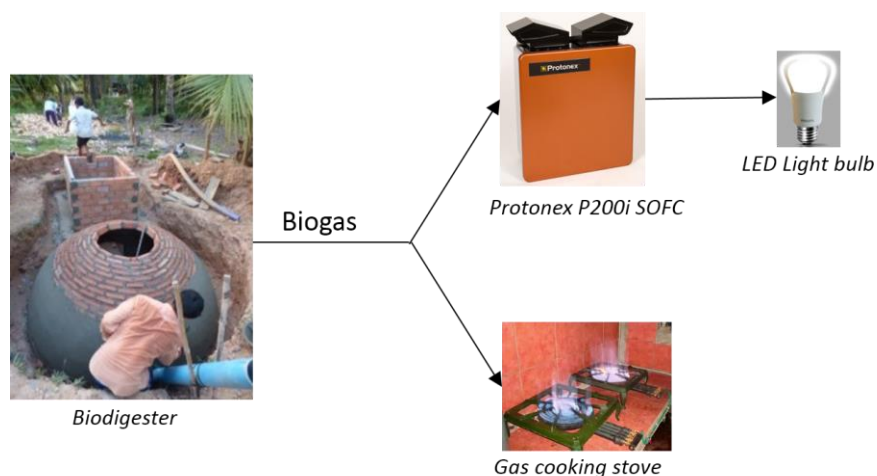


**Figure 2: Biodigester-SOFC system flow chart.**

The high operating temperature of SOFC provides both advantages and challenges. The former include high efficiency and direct electro-oxidation of  $C_1$  ( $CO$ ,  $CH_4$ ) molecules at the anode (McIntosh and Gorte, 2004). The latter include sealing, thermal mismatch, interconnect, and other material and hardware issues. In fact, the chemistry at the anode is far from certain. Thus,

depending upon the anode thickness and the amount of Ni present in the anode cermet layer, *in situ* reforming of simple C<sub>1</sub> fuels such as CH<sub>4</sub> occurs, along with water-gas shift reaction, because of internal recirculation of the water produced via H<sub>2</sub> electro-oxidation (Hecht et al., 2005).

The two most common SOFC structures are tubular and planar. The tubular SOFC (T-SOFC) is typically stronger than the planar cell in terms of ability to handle both thermal and mechanical stress. T-SOFC are also advantageous over planar SOFC due to their sealing capabilities. The ratio of active area to sealing area for a T-SOFC is much greater than that of a planar SOFC, decreasing the risk of leaks at the site of sealing (Waldemar et al., 2007). Figure 3 shows typical tubular solid oxide fuel cells.



*Figure 3: Typical tubular solid oxide fuel cells (Tubular, n.d.).*

Despite the apparent feasibility of a direct biogas-fed SOFC, there is often concern over carbon deposition at the anode. Carbon deposition is detrimental to SOFC because the solid carbon deactivates the Ni catalyst by inhibiting the transport of reactants and of electrons at the Ni surface and can also destroy the anode structure. Thermodynamic analyses have been performed to determine the possibility of carbon deposition based on fuel composition and operating temperature. According to Shiratori et al.'s (2010) work on internal dry reforming of biogas

mixtures, a SOFC fed with a biogas mixture of 50% CH<sub>4</sub>:50% CO<sub>2</sub> should operate around at least 900°C to prevent carbon deposition (Shiratori et al., 2010). The high temperature operation of hydrocarbon-fed SOFCs leads to a high cost of operation. To combat this high cost, research has been done on external reformation where hydrogen is extracted from the hydrocarbon fuel before entering the cell. Doing so protects the anode from carbon deposition while allowing lower operating temperatures. This strategy is effective in decreasing the cost associated with high-temperature operation, but there are costs associated with external reforming equipment and operation as well, and the efficiency of the cell is reduced when externally reforming the fuel. Due to these significant drawbacks with low-temperature operation coupled with external reforming, the focus of this work is a direct biogas SOFC with a high-temperature operation and internal reforming.

Previous research has been conducted on the performance of SOFC running on internally reformed synthetic biogas; however, most of the research is done on small-scale planar button cells that produce power on the milliwatt scale. For example, a 64 mm<sup>2</sup> planar cell operated for 800 hours and produced approximately 100 milliwatts for the duration of the test (Shiratori et al., 2010). Two cells, 60 mm<sup>2</sup> and 80 mm<sup>2</sup> planar cells, were run for about 500 hours each and produced around 15 and 60 watts for each size cell, respectively (Papadam et al., 2012).

Although both groups obtained results that show the potential of SOFC operating on biogas, button cell research is limited due to the smaller active area of the cell, as well as the lack of a concentration gradient over the length of the cell (*Standardization*, n.d.), causing the results of the button cell research to be not directly applicable to large-scale SOFC in commercial SOFC systems. The work performed in this research aims to bridge the gap between the current

research on small milliwatt-scale fuel cells and larger watt-scale fuel cells that have the potential to be used in a commercially available SOFC system.

The following chapters include a review of related literature, methodology, results and discussion, and conclusions. The literature review provides information about both the biogas and fuel cell industries, and what research has been done thus far to merge the two industries. The methodology details the methods used to obtain results for the following five objectives:

1. Determine the effects of biogas composition on performance of single SOFC
2. Determine the effects of fuel utilization on lifetime of single SOFC
3. Determine the effects of moisture in feed on SOFC lifetime
4. Analyze the outlet gas composition of single SOFC with mass spectrometer
5. Operate a 5-cell SOFC assembly on synthetic biogas

The results and discussion chapter is broken up based on each of the above objectives. The conclusions summarize the main findings, and include a discussion of the commercialization potential of the biogas-fed SOFC studied in this experiment.

## 2. Literature Review

To contextualize the issues motivating this project, the literature review here will provide information about fuel cells and their capabilities, especially in the biofuel industry. The chapter will begin with an overview of the world's current energy usage and production, and its effects on the environment. The chapter then will explain the technical aspects of both solid oxide fuel cells and biogas. Finally, to provide context for how the work presented in this report fits in to the current state of the art, the literature review will couple the SOFC and biogas discussion by summarizing research that has previously been done on feeding biogas through SOFCs.

### 2.1 Fuel Cells as an Energy-Producing Technology

In a world where the demand for energy is rapidly increasing, discovering clean energy sources and developing efficient technology to use those resources is critical. Discovered by William Robert Grove, the “gas battery,” or fuel cell, took off in 1840 when Grove found that he could generate an electric current by reversing the hydrolysis of water (SAE, 2015). Since then, fuel cells have been used and tested by NASA on spacecraft, leading car manufacturers, the US military, and many other industries in an attempt to efficiently produce clean energy. The fuel cell industry is projected to continue to grow with an industry value of \$5.20 billion by 2019. Further, the number of stationary, portable, and transportation fuel cell shipments is expected to exceed 200,000 by 2019 (Figure 4)(*Fuel Cell Technology*, 2014).

#### 2.1.1 Global Energy Status

Energy serves as the foundation for a healthy global economy, providing essential services for humans around the world. Many countries desire access to energy resources and the technology that enables them to utilize those resources efficiently in order to improve their economy and

residents' quality of lives. Currently, coal, oil, and natural gas (fossil fuels) are the world's primary sources of energy accounting for about 75% of the world's total energy supply. When burned, however, these fossil energy sources produces the greenhouse gas carbon dioxide (CO<sub>2</sub>), along with pollutants such as carbon monoxide (CO) and nitrogen oxides (NO<sub>x</sub>), leading to high levels of air pollution (Bond and Templeton, 2011).

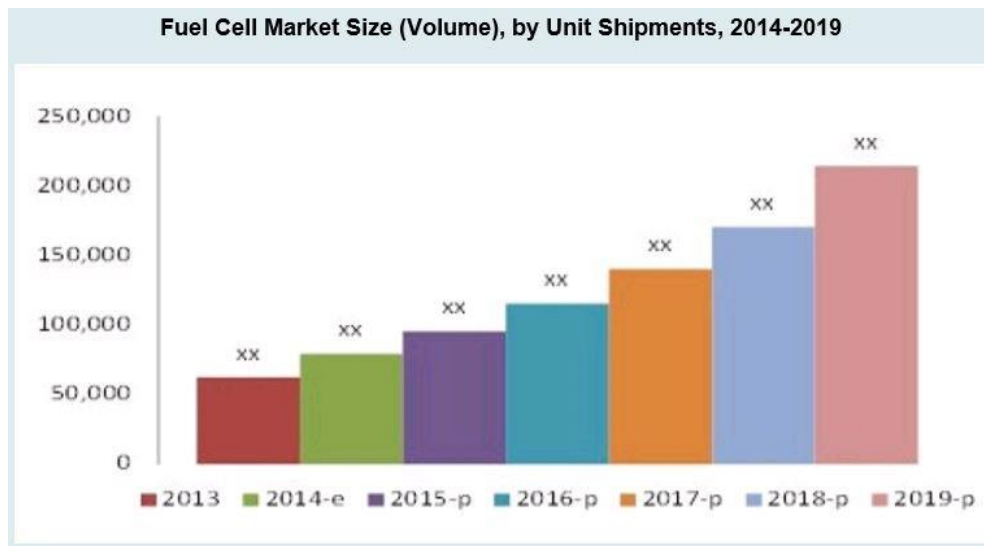


*Figure 4: Fuel cell market size projection (Fuel Cell Technology, 2014).*

The planet's population is continually increasing and expected to reach nine billion people by 2050 (Population, n.d.), as is their standard of living. These two factors together naturally give rise to an increasing energy demand for the foreseeable future. The fossil fuel supply is limited, so continued use without greatly increasing the renewable fuel options could lead to a depletion of the world's energy supply while adding to greenhouse gas emissions, a worrisome scenario for the global economy and climate change. If renewable resources and technologies are not increasingly utilized, the increasing energy demand has the potential to outweigh the finite fossil fuel supply, creating a global energy crisis (FAO, n.d.).

### *2.1.2 Fuel Cell Operation*

Fuel cell technology mitigates the harmful emissions of current energy-producing methods by producing energy more efficiently and therefore with smaller net quantities of CO<sub>2</sub> and CO emissions. This technology converts the chemical energy present in hydrogen-rich fuels directly into electrical energy and utilizable heat, unlike conventional methods, where the energy of a fuel is first converted to thermal energy via combustion, and then into mechanical energy of a turbine, and finally into electrical energy via an alternator. Fuel cells generally consist of anode where the fuel reacts electrocatalytically producing electrons that are directed to the external circuit, and cathode electrodes where the oxidant, usually oxygen from air, gets reduced using the electrons arriving from the external circuit after performing useful work, and an electrolyte separating the two electrodes which allows ions produced at the anode or cathode to complete the circuit.

Other fuels aside from hydrogen may still be used in fuel cells, but some types of fuel cells require external reforming to convert the non-hydrogen fuel to pure hydrogen or a hydrogen rich mixture before entering the cell. In all cases, as long as there is fuel and oxygen supply, fuel cells produce electricity, and thus, unlike batteries, they do not require recharging (Fuel Cell Energy, n.d.).

### *2.1.3 Types of Fuel Cells*

There are many different types of fuel cells being researched today. Most of the cells are named by their electrolyte characteristics. Examples include polymer electrolyte fuel cells (PEMFC), alkaline fuel cells (AFC), phosphoric acid fuel cells (PAFC), molten carbonate fuel cells (MCFC), and solid oxide fuel cells (SOFC). This section will discuss the basic characteristics of these 5 types of fuel cells and their advantages and disadvantages (U.S.D.O.E, 2004).

The first type of fuel cell that will be discussed is the polymer electrolyte fuel cell (PEMFC). The electrolyte for this type of fuel cell is the ion exchange membrane, which is a solid electrolyte that conducts protons. This electrolyte requires constant hydration, so the water in the cell must not evaporate faster than it is produced. This restriction imposes a strict operating temperature range of 60°C-100°C, with most cells operating between 60°C and 80°C. This also means that pure H<sub>2</sub> is required as a fuel with very low tolerance for CO, which poisons the catalyst. The anode and cathode catalyst for the PEMFC is generally a platinum-based catalyst. The general operation of the PEMFC/PAFC is shown in Figure 5 (U.S. D.O.E., 2004). The PAFC instead utilizes supported phosphoric acid as the electrolyte and operates at higher temperatures (150 – 220 °C) and so can utilize reformed hydrogen with up to 1% CO directly.

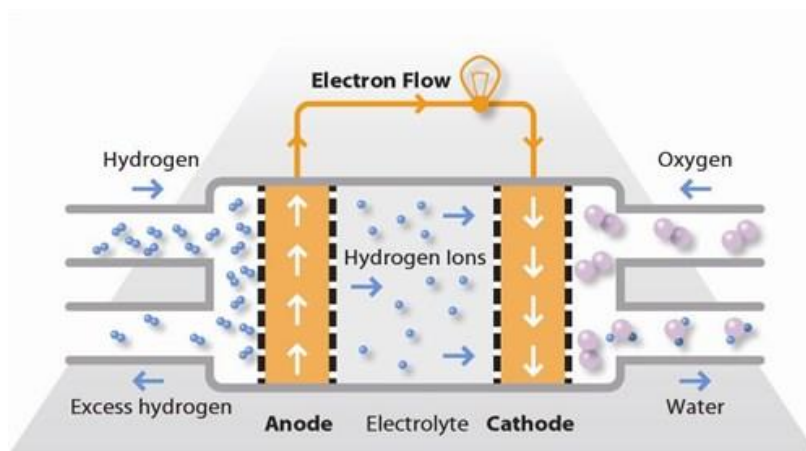


*Figure 5: Operation of PEMFC or PAFC (Technologies, 2016).*

The most common application for PEMFC is in the fuel cell vehicle (FCV) industry. There is also PEMFC presence in portable power and small stationary power (U.S. D.O.E., 2004) The most prominent limiter to additional commercialization of PEMFC is the cost and durability. The components of a PEMFC are inherently expensive and undergo significant degradation after about 5,000 hours for lightweight vehicles, and 40,000 hours for small stationary power systems.

The Department of Energy (DOE) consistently establishes goals to decrease the loading of the platinum catalyst in the PEMFC, as well as the overall cost to increase its commercialization potential (Wang et al., 2011).

Overall, there are many advantages to PEMFC. One of these includes fast start-up due to the low operating temperature. Also, the performance in terms of current and power density is very high. On the other hand, there are a few disadvantages to PAFC as well. The low operating temperature only allows the use of hydrogen rather than commercially available fuels. Any contaminants including CO, sulfur, and ammonia are detrimental to the performance of the cell. In addition, there is currently a lack of hydrogen infrastructure available (U.S. D.O.E., 2004), and hydrogen, being the lightest element is difficult to efficiently transport and store.

The phosphoric acid fuel cell (PAFC) uses a liquid phosphoric acid as its electrolyte. The acid is generally concentrated at 100 percent and operates around 150°C-220°. The anode and cathode are made of a porous carbon material with a platinum catalyst. The operation of PAFCs is identical to that of the PEMFC shown in Figure 5 above.

The efficiency of PAFCs are very high at 85 percent when factoring in electricity plus heat, but for just electricity, the efficiency is about 37-42 percent, which is only slightly more than that of a combustion-based conventional heat engine generator. PAFCs have many advantages over other fuel cells. They have a higher tolerance than PEMFCs and AFCs for small amounts of impurities such as CO, but their low operating temperature still allows for the use of common and commercially available materials. In addition, PAFCs produce a significant amount of usable waste heat. There are some disadvantages of PAFCs though. One of these includes the fact that the phosphoric acid electrolyte is very corrosive, so expensive separators are required in the

stack. Also, efficient PAFCs still require expensive and complex reformer systems including a water gas shift reactor when methane is used as the fuel.

Another type of fuel cell is the alkaline fuel cell (AFC). The AFC uses a potassium hydroxide (KOH) electrolyte soaked into a porous separator. If the cell is operated at high temperatures, above 250°C, the KOH is concentrated at about 85 wt. percent. If the AFC is operated at lower temperatures, less than 120°C, the KOH is less concentrated at about 35-50 wt. percent. The AFC can use a variety of catalysts including nickel, silver, metal oxides, spinels, and noble metals (U.S. D.O.E., 2004), although Pt is still the most common catalyst employed. The operation of an AFC is depicted in Figure 6.

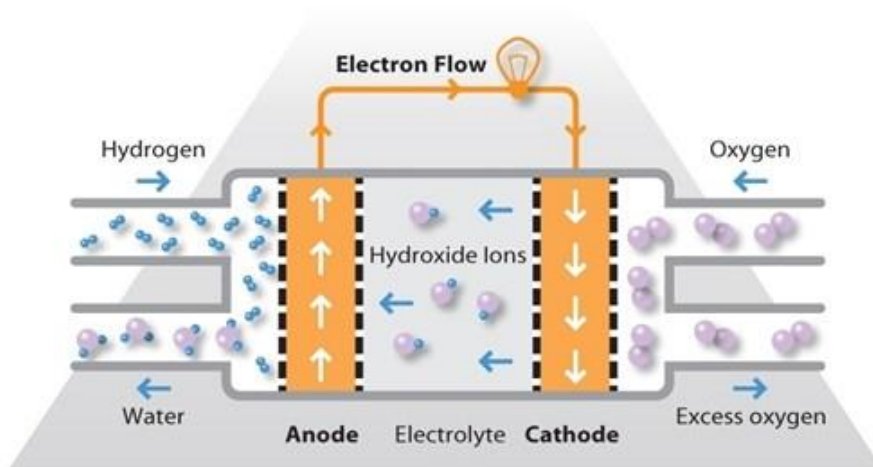


*Figure 6: Operation of AFC (Technologies, 2016).*

The AFC was one of the first fuel cells to be developed. They were developed with a goal of using them on the Apollo space mission to provide electricity as well as potable water on the space craft. Unfortunately, for terrestrial applications the AFC is very susceptible to CO<sub>2</sub> poisoning, even at very small concentrations such as those in the air, and the CO<sub>2</sub> can negatively affect the performance and lifetime of the fuel cell by reacting with the KOH electrolyte. One of

the advantages of the AFC is the high rate at which the electrochemical reactions, hydrogen oxidation reaction (HOR) at the anode, as well as oxygen reduction reaction (ORR) at the cathode, occur due to the variety of suitable catalysts. When pure hydrogen and oxygen are used, the AFC can achieve up to 60% efficiency. Despite the potential of the AFC, the CO<sub>2</sub> intolerance requires an extremely precise removal system, an aspect that can significantly increase the cost and size of an AFC system.

The electrolyte in the molten carbonate fuel cell (MCFC) generally consists of an alkali carbonate and is operated at high temperatures (600°C-700°C). At these high temperatures, there is no longer a need for expensive precious metal catalysts at the anode and cathode. The typical catalysts for an MCFC are nickel at the anode and nickel oxide at the cathode. Because of the high temperature of operation, the MCFC can utilize fuels other than hydrogen, such as hydrocarbons, natural gas, and biogas. Figure 7 shows the operation of an MCFC.

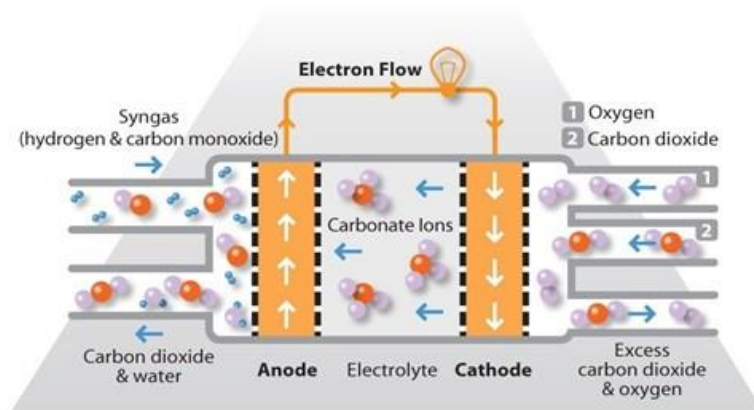


*Figure 7: Operation of MCFC (Technologies, 2016).*

Overall, the advantages of MCFCs include the ability to use inexpensive catalysts and readily available fuels, and being able to recycle the waste heat from the high temperature cell improves the efficiency of the cell to be over 50 percent. One of the major disadvantages of the MCFC is

the corrosiveness of the electrolyte. Also, despite the advantages of the high operating temperature, the high temperatures introduce problems with materials and stability of the system (U.S. D.O.E., 2004).

Solid oxide fuel cells (SOFCs) are a highly efficient power-producing system (about 60% efficiency) (Garrison, n.d.) that operate under very high temperatures (600°C-1000°C), allowing for internal reformation of fuels. Internal reformation allows for more practical fuels than hydrogen to be used directly in the fuel cell because the fuel does not have to go through advanced and expensive external reforming. In addition to oxidizing hydrogen, SOFC has the ability to directly oxidize CO as well (Yi et al., 2005). Figure 8 shows the operation of an SOFC.

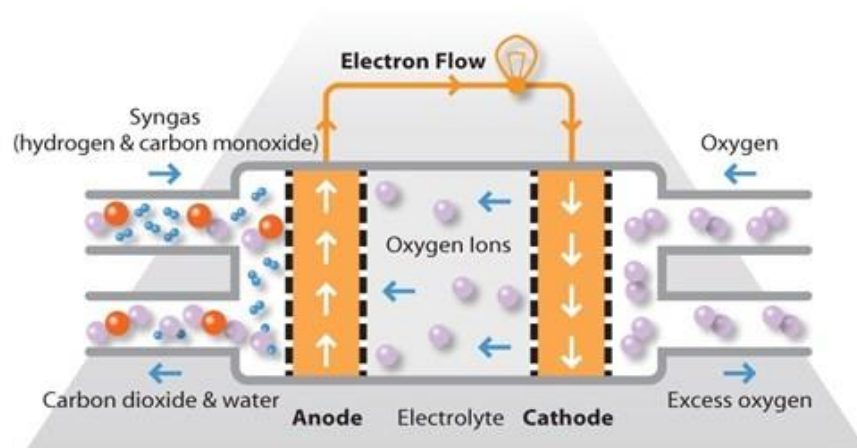


*Figure 8: Operation of SOFC (Technologies, 2016).*

The two most common SOFC structures are tubular and planar. The tubular SOFC (T-SOFC) is typically stronger than the planar cell in terms of ability to handle both thermal and mechanical stress, making the tubular cell an excellent match for small-scale and portable systems (Protonex, n.d.), similar to those that would be implemented alongside biodigesters in small rural communities. A porous Ni-YSZ (nickel-yttria stabilized zirconia) anode is very common in T-

SOFCs. Ni-YSZ is relatively inexpensive, robust in high-temperature atmospheres, and displays similar expansion properties to a YSZ electrolyte. The Ni plays an important role in the functioning of the cell by serving as an electronic conductor and internal reforming catalyst. The reforming characteristic is especially important when hydrocarbons, like CH<sub>4</sub>, are fed directly to the cell, as the Ni acts as a reforming catalyst when H<sub>2</sub>, CO, CO<sub>2</sub> are produced from the CH<sub>4</sub> and H<sub>2</sub>O (Hecht et al., 2005).

The SOFC electrolyte must conduct oxide ions and be dense to prevent the passage of gas molecules. The YSZ electrolyte is a common electrolyte material due to its high oxide ion conductivity and high density, but it is also not highly conductive electronically so that the electronic current does not leak from the interconnects (Hecht et al., 2005).

There are many advantages to using SOFCs including the ability to oxidize CO in the cell, the relatively inexpensive cell materials, and high efficiencies. The disadvantages are generally associated with the high temperature operation of the cell, as the high temperature poses problems with thermal expansion and corrosion of various parts of the stack. There are also difficulties with sealing between planar fuel cells (U.S. D.O.E., 2004).

### *2.1.5 Fuel Cell Performance Modeling*

The three main variables for fuel cell characterization include voltage ( $V$ ), current ( $I$ ) or current density ( $i$ ), and power ( $P$ ) or power density. Voltage and current can be measured during the operation of the fuel cell, and power can be calculated as the product of the voltage and current as shown in equation 1.

$$P = V \times I \quad (1)$$

One of the most common ways to characterize the performance of a fuel cell is either with potentiostatic or galvanostatic techniques. Potentiostatic method involves applying a constant voltage potential to the cell while measuring the responding current. Galvanostatic is the opposite; applying a constant current to the cell while measuring the resulting voltage potential. After conducting an experiment using either of these techniques, a power versus time graph can be constructed based on the product of the current and voltage results. The purpose of this type of characterization is to observe the behavior of the cell over time (Olivier, 2008). Potentiostatic and galvanostatic techniques are especially useful when observing the lifetime of a cell, especially if there is a risk of degradation.

Not only is it beneficial to observe current or voltage over time, but the relationship between current density and voltage can also present useful information. This relationship is usually shown in a polarization curve (Figure 9) where the cell voltage is plotted against the current density, defined as the electric current per cross-sectional area of the cell.

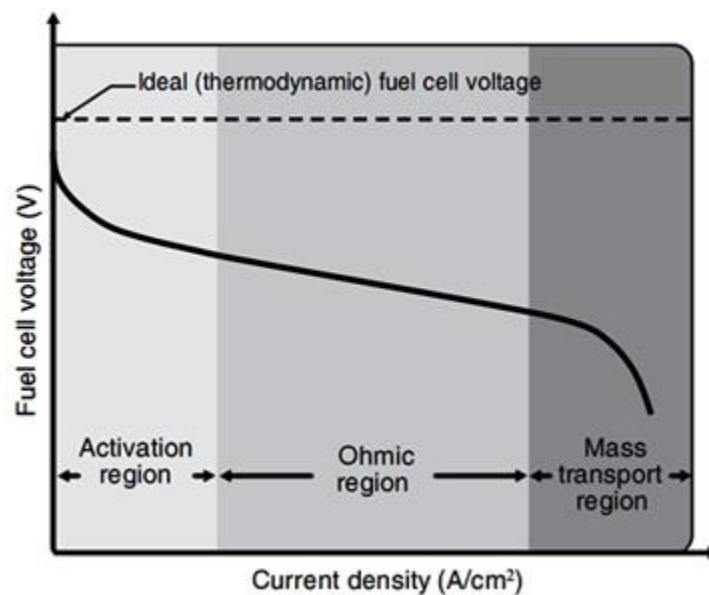


*Figure 9: Plot of low temperature polarization curve with overpotentials (Introduction, 2012).*

Polarization curves are helpful when examining the voltage losses associated with the cell. Figure 9 is an example of a polarization plot for a low temperature fuel cell. The losses associated with high temperature fuel cells are generally small, and the polarization plot is linear. On the other hand, in low temperature fuel cells Tafel or logarithmic dependence is observed between voltage loss and current density for electrode reactions. A fuel cell has an ideal voltage that is constant with respect to the current density and greater than the actual voltage. Any deviation from this constant voltage is called over voltage or over potential, and the difference between the actual voltage and the theoretical voltage is inversely proportional to the cell's power output; that is, the smaller the difference between the voltages the greater the cell's power output (Rayment, 2003).

The anode, cathode, and overall cell reactions for the case of hydrogen fuel flowing through a solid oxide fuel cell are as follows:

| Electrode       | Reaction   | Potential (V)           | $\Delta G_p^o$ (kJ/mol) | $\sigma_p$ |
|-----------------|--|-------------------------|-------------------------|------------|
| <i>Anode:</i>   | $\text{H}_2 + \text{O}^{2-} \rightleftharpoons \text{H}_2\text{O} + 2\text{e}^-$ | $\Phi_{A,0}^o = -0.560$ | -99.5                   | +2         |
| <i>Cathode:</i> | $\text{O}_2 + 4\text{e}^- \rightleftharpoons 2\text{O}^{2-}$                     | $\Phi_{C,0}^o = +0.669$ | -258.2                  | +1         |
| <i>Overall:</i> | $2\text{H}_2 + \text{O}_2 \rightleftharpoons 2\text{H}_2\text{O}(\text{g})$      | $V_0^o = 1.185$         | -457.4                  |            |

(2)

The thermodynamic data and the corresponding electrode potentials are based on assuming that the enthalpy of formation of the oxygen anion in YSZ is  $H_{f,\text{O}^{2-}(\text{YSZ})}^o = -85.6$  kJ/mol, and entropy  $S_{f,\text{O}^{2-}(\text{YSZ})}^o = 148.4$  J/molK (Goodwin et al., 2009), further assumed to be independent of temperature, so that  $G_{f,\text{O}^{2-}(\text{YSZ})}^o = -129.1$  kJ/mol. It is worth mentioning that these thermodynamic parameters are not yet known precisely. The water formed is assumed in the

vapor form, i.e.,  $G_{f,H_2O(g)}^o = -228.6$  kJ/mol. Further, the Gibbs free energy and hence the cell thermodynamic potential declines with temperature, i.e.,

$$V_0 = 1.185 - 2.302 \times 10^{-4}(T - 298) - \frac{RT}{2F} \ln \frac{x_{H_2}^2 x_{O_2}}{x_{H_2O}^2} \quad (3)$$

Similarly, for the case of CO fuel, the anode, cathode, and overall cell reactions are

| Electrode       | Reaction                                     | Potential (V)           | $\Delta G_p^o$ (kJ/mol) | $\sigma_p$ |
|-----------------|--|-------------------------|-------------------------|------------|
| <i>Anode:</i>   | $CO + O^{2-} \rightleftharpoons CO_2 + 2e^-$ | $\Phi_{A,0}^o = -0.664$ | -128.1                  | +2         |
| <i>Cathode:</i> | $O_2 + 4e^- \rightleftharpoons 2O^{2-}$      | $\Phi_{C,0}^o = +0.669$ | -258.2                  | +1         |
| <i>Overall:</i> | $2CO + O_2 \rightleftharpoons 2CO_2$         | $V_0^o = 1.333$         | -514.3                  |            |

And the thermodynamic cell potential in relation to temperature is

$$V_0 = \underbrace{1.333 - 4.494 \times 10^{-4}(T - 298)}_{V_0^o} - \frac{RT}{2F} \ln \frac{x_{CO}^2 x_{O_2}}{x_{CO_2}^2} \quad (5)$$

Thus the cell thermodynamic potential declines linearly with temperature for both hydrogen and carbon monoxide fuel.

At a temperature of 1,000 °C under hydrogen conditions, thus, this provides, for unit activities or pure components, a standard thermodynamic potential  $V_0^o = 0.96$  V. The actual thermodynamic cell voltage is different, as affected by the mole fractions of the species indicated in the expression above. The OCV is usually lower because of any crossover and internal shorting as well. The electrolyte in SOFC possesses some electronic conductivity, causing a loss in cell voltage; however, the electrode kinetics at SOFC temperatures are very rapid, with small

overpotentials. The largest potential losses are often due to the electrolyte layer, or due to diffusion limitations in the electrodes at higher current densities.

The three main types of potential losses that contribute the difference between the actual and theoretical voltages include activation, Ohmic, and mass transport losses. As shown in Figure 9, each of these losses occurs at specific current density regions (Rayment, 2003).

The first type of over voltage is called activation losses. These losses occur because the rates of electrochemical reactions require energy to be enhanced, and at this range of operating conditions any available energy is used to activate these reactions rather than produce voltage. High temperatures generally reduce activation losses. Therefore, lower activation losses are typical for SOFCs due to their high operating temperatures (Rayment, 2003).

Ohmic losses, the second type of over potential, occur due to an Ohmic resistance in the flow of electrons. Ohmic losses are present in any electrical system and occur in the middle region of current densities. One way to decrease Ohmic losses is by using electronically-conductive electrode materials, such as Ni, in the anode, and electrolyte layers with higher ionic conductivity or smaller thickness. In addition to conductive electrodes, the electrodes should be short because distance is proportional to resistance, meaning that resistance is increased with longer electrodes (Rayment, 2003).

The final category of over potential is mass transport loss. This kind of loss occurs due a decreasing partial pressure or concentration of fuel at either the anode or the cathode. At the anode, for example, as the cell uses up the available hydrogen, the partial pressure of hydrogen in the anode decreases, lowering the rate of diffusion and hence the voltage. The same idea is evident with air pressure at the cathode. In the case of biogas, since  $\text{CH}_4$  produces double the

amount of hydrogen than would normally be fed through an SOFC, the mass transfer losses are expected to be minimal due to an excess amount of hydrogen present at the anode (Rayment, 2003).

As an external current is drawn, as when experimentally producing a polarization curve, the reduction in potential registered  $V$  is equal to  $V_0$  minus the sum of the potential drops overpotentials across all the internal components in series, namely, anode, electrolyte, cathode, and gas-diffusion layer. Equation 6 shows the relationship between the local current density, the potential drops, and the resulting overall cell potential (Janardhanan and Deutschmann, 2007)

$$V = V_0 - \eta_a(i) - |\eta_c(i)| - \eta_{ohm}(i) - \eta_{conc}(i) \quad (6)$$

The anode and cathode (represented respectively by the subscripts  $a$  and  $c$ ) overpotentials are represented by  $\eta_a$  and  $\eta_c$ , respectively, and can be calculated via equations 7 and 8.

$$\eta_a = \frac{2RT}{n_e F} \sinh^{-1} \left( \frac{i}{2i_{0a}} \right) \quad (7)$$

$$\eta_c = \frac{2RT}{n_e F} \sinh^{-1} \left( \frac{i}{2i_{0c}} \right) \quad (8)$$

The local current density is represented by  $i$ , and  $i_{0a}$  and  $i_{0c}$  are the exchange current densities of the anode and cathode respectively.

The Ohmic overpotential ( $\eta_{ohm}$ ) can be calculated with equation 9,

$$\eta_{ohm} = iR_{tot} \quad (9)$$

where  $R_{tot}$ , the total resistance of all of the cell components, can be calculated by equation 10.

$$R_{tot} = \rho_e l_e + \rho_a l_a + \rho_c l_c + R_{contact} \quad (10)$$

In equation 13, the subscript e represents the electrolyte,  $\rho$  is the specific electrical resistance of the cell component (electrolyte, anode, and cathode),  $l$  is the component's thickness, and  $R_{contact}$  is the contact resistance, if any.

The final loss category represented in equation 6 is concentration loss, or  $\eta_{conc}$ . The concentration loss can be calculated using equation 11,

$$\eta_{conc} = \frac{RT}{n_e F} \ln \left( 1 - \frac{i}{i_l} \right) \quad (11)$$

where  $i_l$  is the limiting current density, when the current is limited completely by diffusional limitations of the reactant. Figure 10 presents a polarization plot for the case of pure H<sub>2</sub> and pure CO fed to a SOFC.

For the case of pure hydrogen, the standard cell potential,  $V_0$ , can be described by equation 6, and thus, after calculating the losses throughout the cell (equations 7-11), the potential with respect to any current density can be calculated using equation 9. This calculation would allow for the creation of a theoretical polarization plot for pure H<sub>2</sub>. A similar method could be used for pure CO.

Polarization plots for pure H<sub>2</sub> and CO fed SOFC have been provided in the literature, and an example of one generated at 850 °C is shown in Figure 10. In addition to the voltage versus current curve, power versus current density is commonly plotted as well. It is clear from this that SOFC, owing to its high operating temperatures, is fully capable to electrocatalytically oxidizing CO directly, while it acts as a poison for the lower temperature fuel cells, which are unable to electrochemically oxidize CO. Further, the polarization plot for CO is only slightly lower than that for H<sub>2</sub>, indicating a key advantage of the high temperature operation of the SOFC. Electrode kinetics are enhanced by both temperature and by potential as described by the Arrhenius and the

Butler-Volmer equations, respectively. Therefore, temperature and potential are complementary. A high operating temperature means lower overpotentials or kinetic potential losses.

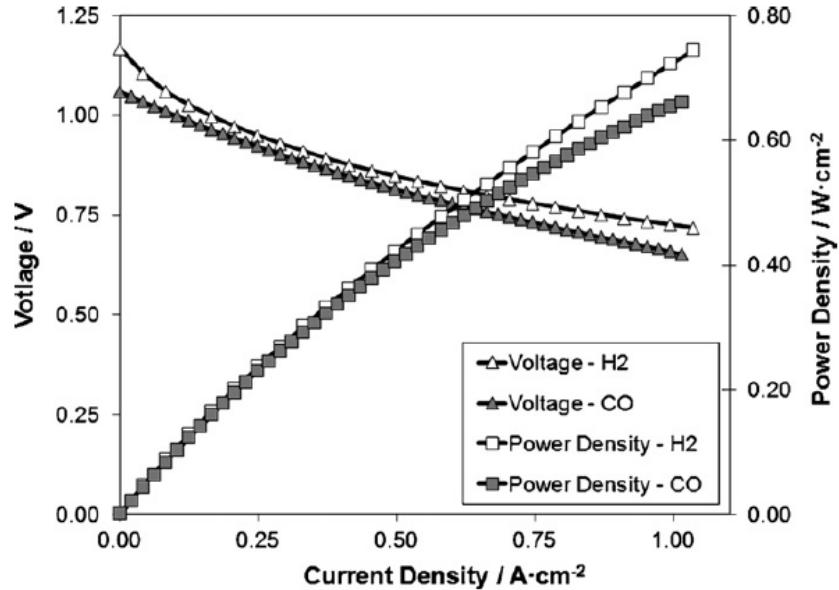


*Figure 10: Polarization plot for pure hydrogen and CO with power density (Homel et al., 2010).*

## 2.2 Harnessing Biogas

Carbon dioxide (CO<sub>2</sub>) and methane (CH<sub>4</sub>) are the two main components of biogas formed from the anaerobic fermentation of organic waste. As a greenhouse gas, methane is actually 25 times more damaging to the atmosphere than CO<sub>2</sub>. In terms of CO<sub>2</sub> equivalence over 6,000 million metric tons of methane were released into the atmosphere in 2013 (EPA, n.d.). However, methane can be harnessed using effective technology and used as a fuel. Ever since 1970 when the Chinese government “promoted biogas use in every rural family” and facilitated the installation of over 7 million biodigesters, about 42 million small-scale household biodigesters have been built in China and about 4 million in India in an effort to harness biogas. The biogas is typically used for cooking, lighting, and sometimes with small combustion engines (Bond and Templeton, 2011). Figure 11 shows this process being utilized in Vietnam.



*Figure 11: Biodigester to cooking stove process (Tahezadeh, 2012).*

Organic waste consists of any biodegradable waste from plants, animals, or humans. There are three possible paths for this waste. One is for the  $\text{CO}_2$  and  $\text{CH}_4$  emissions to be released to the atmosphere and contribute to an increase in greenhouse gas emissions. The second path is for biogas to be burned and used for heating/cooking, while the third is to be used as a fuel in a fuel cell to generate power.

A biodigester is the vessel where organic waste undergoes anaerobic digestion to produce biogas. Biogas consists of mostly  $\text{CH}_4$  and  $\text{CO}_2$ , and traces of water vapor ( $\text{H}_2\text{O}$ ), hydrogen sulfide ( $\text{H}_2\text{S}$ ),  $\text{CO}$ , and nitrogen gas ( $\text{N}_2$ ). Figure 12 shows the biochemical process of anaerobic digestion.

Some of the most common feedstocks include agricultural residue, food waste, and animal byproducts (manure, etc.). In general, the  $\text{CH}_4$  content in the biogas produced from any kind of feedstock ranges between 50-80%. This is a large range because there are many factors that influence the biogas content. One factor is the characteristics of the feedstock. Within the food waste category, carbohydrates, fats, and proteins produce about 50%, 70%, and 60%  $\text{CH}_4$ ,

respectively (Muzenda, 2014). If a biodigester were to be fed with food waste, the composition of the biogas would range between 50-70% CH<sub>4</sub> depending on the biochemical characteristics of the waste. In terms of manure, the contents of manure vary depending on the diet of the animal. Dairy cattle manure, for example, produces biogas with 62% CH<sub>4</sub> content, however, beef cattle produces biogas with 56% CH<sub>4</sub> (Cropgen, n.d.). In addition, current research has been focused on codigestion, where one biodigester operates on different kinds of biowastes (e.g. manure + food mixtures). El-Mashad et al. (2010) showed that this method increases biogas and CH<sub>4</sub> production (Table 1); however, it introduces additional variability in the feedstock, and thus, the additional variability in the CH<sub>4</sub> content of the biogas (El-Mashad and Zhang, 2010).

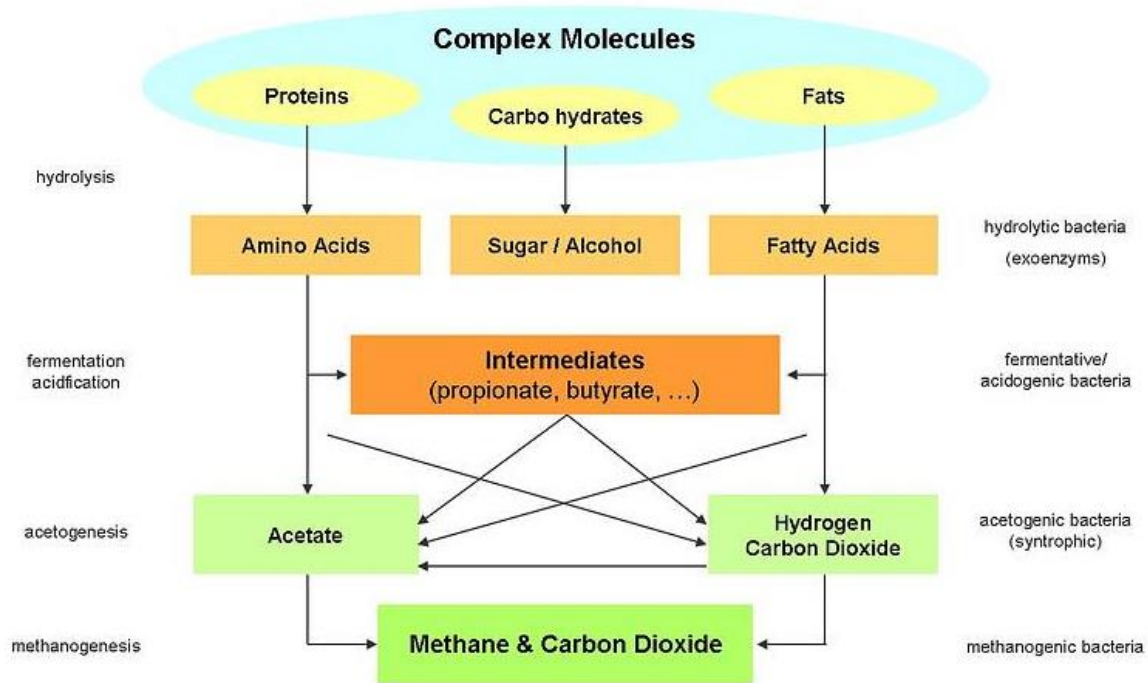


*Figure 12: Biochemical process of anaerobic digestion (Anaerobic, n.d.).*

Another cause of inconsistent biogas content is temperature changes. Vindis and Mursec (2009) performed an experiment on the effect of mesophilic (35-37°C) versus thermophilic (55-60°C)

biodigester temperatures on the CH<sub>4</sub> content of the biogas produced from a variety of maize feedstocks (Figure 13) (Vindis and Mursec, 2009).

*Table 1: The effect of co-digestion on methane production in biogas (El-Mashad and Zhang, 2010).*

| Mixtures, food waste % + manure % | Predicted methane yield (L/kgVS fed) |         |
|-----------------------------------|--------------------------------------|---------|
|                                   | 20 days                              | 30 days |
| 10% + 90%                         | 178                                  | 211     |
| 20% + 80%                         | 205                                  | 235     |
| 32% + 68%                         | 235                                  | 262     |
| 40% + 60%                         | 255                                  | 280     |
| 48% + 52%                         | 274                                  | 298     |
| 60% + 40%                         | 301                                  | 323     |
| 70% + 30%                         | 322                                  | 344     |
| 80% + 20%                         | 342                                  | 365     |
| 90% + 10%                         | 361                                  | 385     |

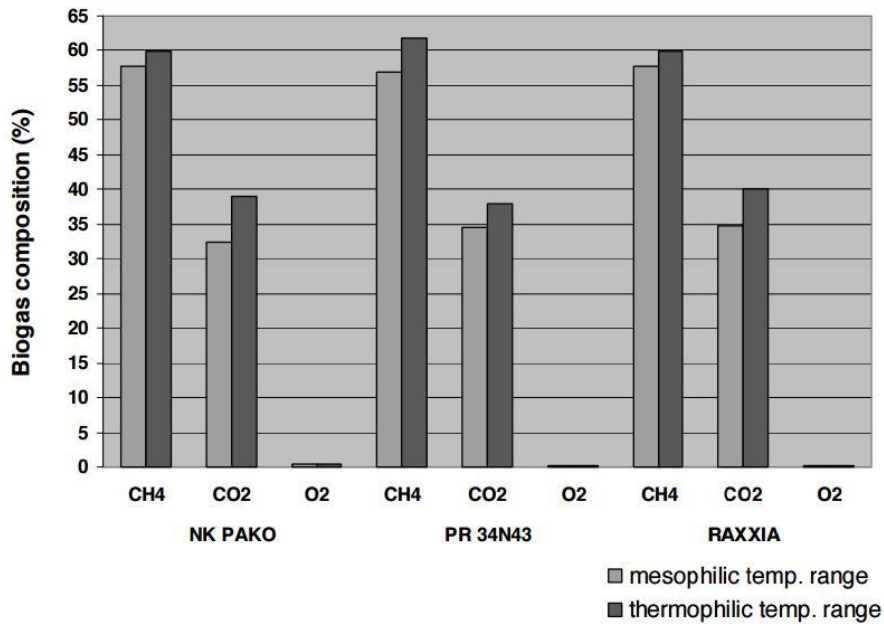
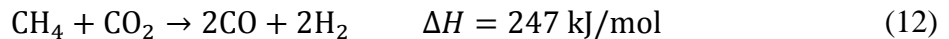


*Figure 13: Effect of temperature on methane production (Vindis and Mursec, 2009).*

The results of this study showed that the average CH<sub>4</sub> content from the mesophilic reactor was 57% and the average CH<sub>4</sub> content from the thermophilic reactor was 60.5% (Vindis and Mursec, 2009).

### 2.3 Pairing Biogas with SOFCs

Despite the variations that exist in the CH<sub>4</sub> content of biogas, the biogas can be fed to an SOFC to produce power. In order to obtain power from biogas in a SOFC, however, the CH<sub>4</sub> needs to somehow be first converted to H<sub>2</sub> and CO. This can be done via either external or internal reformation. External reformation is a way to convert the CH<sub>4</sub> and CO<sub>2</sub> to H<sub>2</sub>/CO before the fuel enters the cell. This method protects the cell from damage from impurities in the fuel. Despite this protection, external reformation is a costly procedure and decreases the utilization potential of the fuel. This limitation leads to the desire for internal reformation, where the fuel is converted to H<sub>2</sub>/CO within the cell. In the case of an SOFC, internal reformation can occur readily because of its high operating temperature and the presence of the Ni catalyst. Thus, CH<sub>4</sub> and CO<sub>2</sub> in the biogas reform internally at temperatures above 650°C to form H<sub>2</sub> and CO



In the SOFC, the H<sub>2</sub> reacts with the O<sup>2-</sup> to form H<sub>2</sub>O, while the CO reacts with the O<sup>2-</sup> to form CO<sub>2</sub>, as described in Chapter 2, and the resulting electrical current produces a useful voltage. Based on this hypothesis, biogas, in theory, is a suitable feed for an SOFC.

Lanzini et al. (2013) confirmed this theory experimentally by showing that as temperature increased above about 500°C the conversion of CO<sub>2</sub> and CH<sub>4</sub> increased due to enhanced kinetics, producing more CO and H<sub>2</sub> (Figure 14) (Lanzini et al., 2013). At around 850°C, however, the conversion plateaued suggesting that maximum conversion of CH<sub>4</sub> and CO<sub>2</sub> occurs at temperatures around 850°C (Lanzini et al., 2013), conceivably because of thermodynamic limitations. This is discussed in more detail later on in this report.

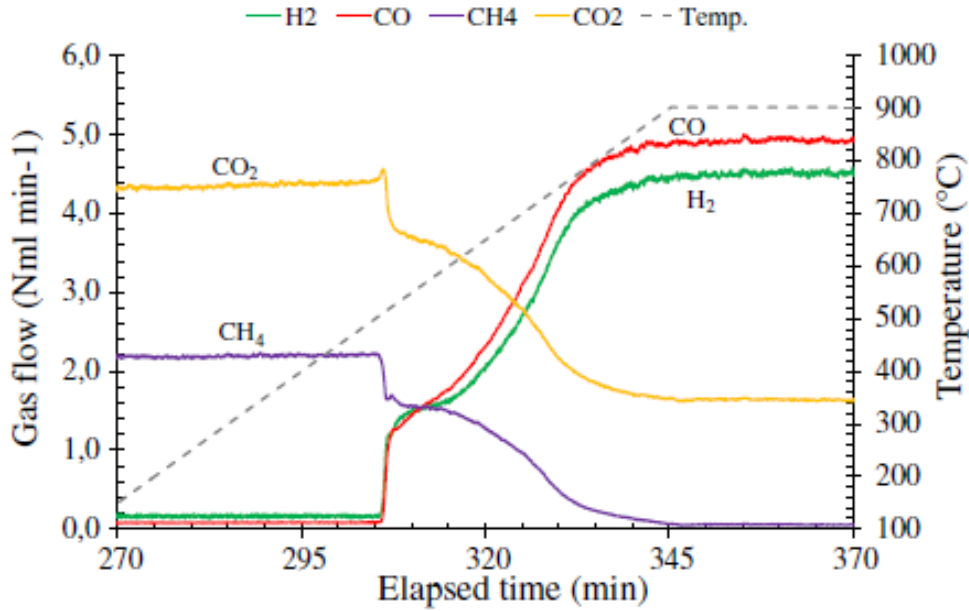


*Figure 14: Temperature effect on biogas conversion (Lanzini et al., 2013).*

### 2.3.1 Carbon Deposition Damaging the SOFC Anode

Despite the apparent feasibility of a direct biogas-fed SOFC, there is a major concern over carbon deposition at the anode. The occurrence of one or more of the following three reactions is possible whenever hydrocarbons or CO are fed through an SOFC:



Carbon deposition is detrimental to an SOFC because the solid carbon inhibits the transfer of reactants and electrons across the Ni surface of the anode, and also possibly dislodges the Ni particles from the anode matrix. Thermodynamic analyses have been performed to determine the possibility of carbon deposition based on fuel composition and reaction temperature.

Assabumrungrat et al. (2006) showed that as the ratio of  $\text{CH}_4:\text{CO}_2$  entering the cell increased, the

carbon activity also increased. This trend occurred at 900K, 950K, 1000K, 1050K, and 1100K, but if the carbon activity were to remain constant at 900K and 1100K, there would be a higher tolerance for a greater CH<sub>4</sub>:CO<sub>2</sub> ratio at 1100K than 900K, suggesting that a higher operating temperature decreases the amount of carbon deposition (Assabumrungrat et al., 2006).

For the case of pure methane, on the other hand, Lanzini et al. (2013) observed how temperature affected carbon deposition on a Ni-YSZ anode support by flowing pure methane through the anode, varying the temperature, and measuring the outlet oxygen, CO<sub>2</sub>, and CO concentrations, as well as the amount of carbon on the anode. As shown in Figure 15, the results of this study suggest at higher temperatures (above 500°C), methane was more likely to form carbon deposits than at the lower temperatures (Lanzini et al., 2013).

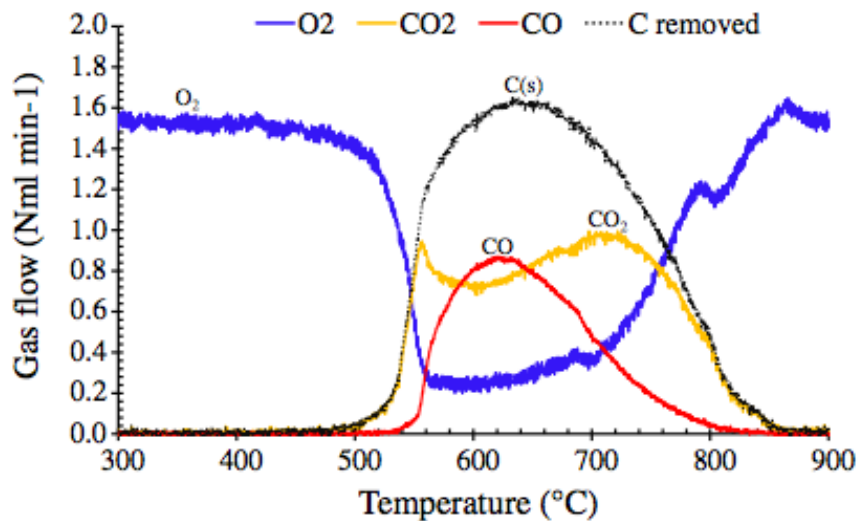


*Figure 15: Temperature effect on carbon deposition (Lanzini et al., 2013).*

Clearly, the presence of CO<sub>2</sub> along with methane in biogas affects the formation of coke.

For the case of pure methane feed, the rate of carbon formation by the carbon deposition reaction (equation 14) can be represented by (Fogler, 2008),

$$r_C = \vec{k}P_{CH_4} - \bar{k}P_{H_2}^2 \alpha_C \quad (16)$$

where  $r_C$  is the rate of carbon formation,  $\vec{k}$  and  $\bar{k}$  are the forward and reverse rate constants, respectively,  $P_i$  is the partial pressure of the associated species, and  $\alpha_i$  is the activity of the associated species. If the activity of carbon is assumed to be equal to 1, the equation for the rate of carbon deposition can be written in terms of the overall rate constant as follows,

$$r_C = \vec{k}P_{CH_4} \left( 1 - \frac{1}{K} \frac{P_{H_2}^2}{P_{CH_4}} \right) \quad (17)$$

where  $K$  is the overall equilibrium constant.

As mentioned above, Lanzini et al. (2013) also observed that at higher temperatures the conversion of  $CH_4$  and  $CO_2$  was greater, leaving almost zero  $CH_4$  (Figure 15). When there is very little  $CH_4$  there is no threat of carbon formation from  $CH_4$  pyrolysis at high temperatures. When there is  $CH_4$  present, however, there is potential for carbon formation as shown in Figure 15. Theoretically, as long as the temperature is high enough to promote 100% conversion of  $CH_4$ , then there is no threat of carbon deposition due to  $CH_4$  pyrolysis (Lanzini et al., 2013).

The high temperature operation of hydrocarbon-fed SOFCs leads to a high cost of operation. To combat this high cost, research has been done on external reformation where hydrogen is extracted from the hydrocarbon fuel before entering the cell. Doing so protects the anode from carbon deposition while allowing lower operating temperatures. This strategy is effective in decreasing the cost associated with high-temperature operation, but there are additional costs associated with external reforming as well, and the efficiency of the cell is reduced when externally reforming the fuel. Due to these significant drawbacks with low-temperature operation

and external reforming, attention will be given to high-temperature operation and internal reforming in this research.

### 2.3.2 Higher Current Density Decreases Carbon Deposition

In order to have internal reforming of the biogas, the conditions must be ideal, causing very little carbon deposition on the anode. Many researchers have claimed anode failure to be due to carbon deposition, and because of this threat, much research has been done on internal steam reforming. Internal steam reforming is beneficial to the cell in a couple ways. First, any excess  $\text{CH}_4$  entering the cell can react with  $\text{H}_2\text{O}$  and form  $\text{CO}$  and  $\text{H}_2$ , two species that are readily electrochemically oxidized in a SOFC. This reaction prevents any excess  $\text{CH}_4$  from breaking down into  $\text{C}$  and  $\text{H}_2$ . Secondly, the water present in the cell can also clean out any carbon that has been deposited on the anode. Laosiripojana and Assabumrungrat (2007) experimentally demonstrated this idea by measuring the amount of carbon formation (monolayers) present after running an SOFC on various  $\text{CH}_4:\text{H}_2\text{O}$  ratios (Table 2) (Laosiripojana and Assabumrungrat, 2007).

**Table 2: Carbon formation with various fuel:water ratios (Laosiripojana and Assabumrungrat, 2007).**

| Type of fuel | Fuel/ $\text{H}_2\text{O}$ ratio | Yield of $\text{H}_2$ production (%) | Fraction of the by-products (%) |               |               |                        |                        | C formation (monolayers) |
|--------------|----------------------------------|--------------------------------------|---------------------------------|---------------|---------------|------------------------|------------------------|--------------------------|
|              |                                  |                                      | CO                              | $\text{CO}_2$ | $\text{CH}_4$ | $\text{C}_2\text{H}_6$ | $\text{C}_2\text{H}_4$ |                          |
| Methane      | 1.0/3.0                          | 70.9                                 | 68.1                            | 31.9          | –             | –                      | –                      | 0.21                     |
|              | 1.0/4.0                          | 73.7                                 | 65.2                            | 34.8          | –             | –                      | –                      | 0.15                     |
|              | 1.0/5.0                          | 77.5                                 | 59.3                            | 40.7          | –             | –                      | –                      | 0.09                     |
| Methanol     | 1.0/3.0                          | 59.7                                 | 62.9                            | 27.7          | 9.4           | –                      | –                      | 0.37                     |
|              | 1.0/4.0                          | 64.2                                 | 60.4                            | 30.5          | 9.1           | –                      | –                      | 0.32                     |
|              | 1.0/5.0                          | 66.3                                 | 57.5                            | 33.8          | 8.7           | –                      | –                      | 0.26                     |
| Ethanol      | 1.0/3.0                          | 58.3                                 | 44.5                            | 11.8          | 30.2          | 4.7                    | 8.8                    | 4.29                     |
|              | 1.0/4.0                          | 60.0                                 | 42.9                            | 14.9          | 29.8          | 4.3                    | 8.1                    | 4.18                     |
|              | 1.0/5.0                          | 61.4                                 | 41.2                            | 18.3          | 29.1          | 3.9                    | 7.5                    | 4.12                     |

Their work showed that of the three CH<sub>4</sub>:H<sub>2</sub>O ratios (1:3, 1:4, 1:5), the 1:5 ratio produced the least amount of carbon, suggesting that the increase in steam in the cell decreased the presence of carbon in the cell (Laosiripojana and Assabumrungrat, 2007).

It is predicted that running the cell at higher current densities will decrease the presence of carbon in the cell for two reasons. First, by increasing the current density, the partial pressure of steam in the cell also increases because more hydrogen is being oxidized and generating water according to equation 2 above. Kinetically, the oxidation of H<sub>2</sub> and CO occurs before the oxidation of carbon, but Mermelstein et al. (2011) experimentally demonstrated that less carbon deposition was found in the cell when running a cell on higher current density (Figure 16), suggesting that the carbon can be oxidized as well (Mermelstein et al., 2011).

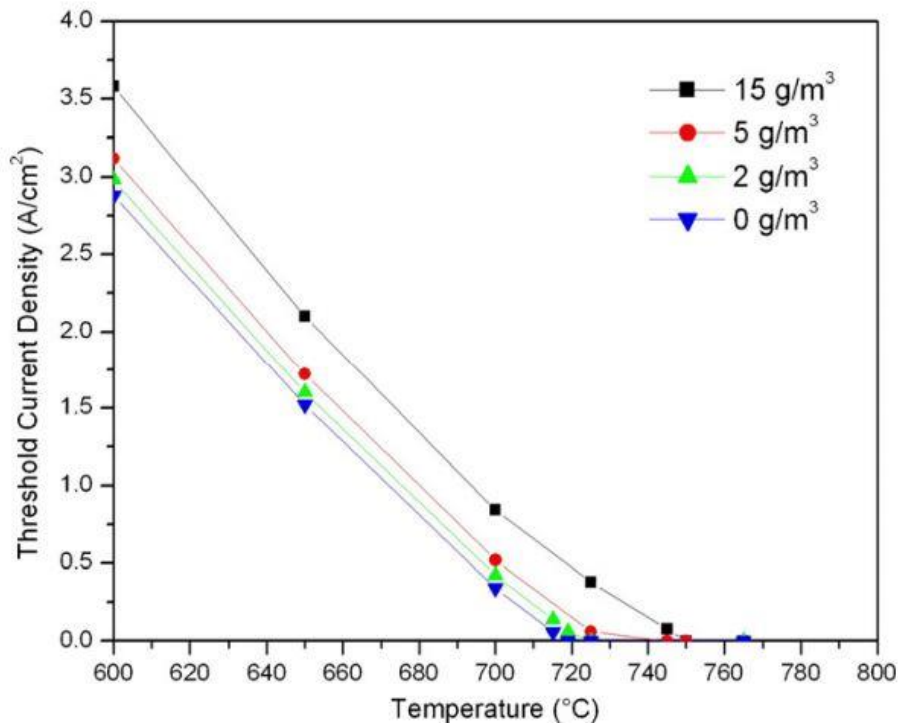


*Figure 16: Current required to suppress various amounts of carbon formation (Mermelstein et al., 2011).*

Running a cell on high current density or under higher partial pressure of water has the potential to promote to steam reforming and oxidization of carbon deposits, and thus decrease the amount of carbon deposition in the cell.

### 2.3.3 Lack of Larger-Scale, Tubular SOFC Research with Biogas

Previous research has been conducted on the performance of SOFCs running on internally reformed synthetic biogas; however, most of the research is done on small-scale planar button cells that produce power on the milliwatt scale. For example, Shiratori et al. (2010) ran a 64 mm<sup>2</sup> planar cell for 800 hours and produced approximately 100 milliwatts for the duration of the test (Figure 17) (Shiratori et al., 2010).

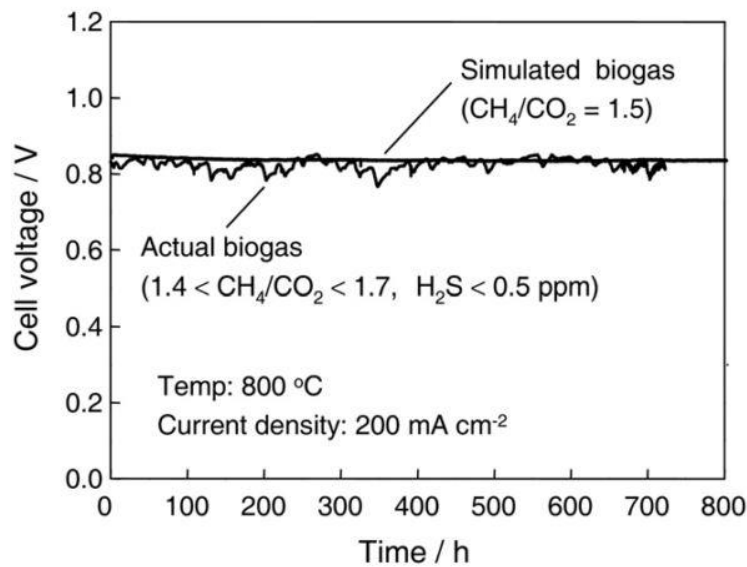


*Figure 17: 800 hour button cell test (Shiratori et al., 2010).*

Papadam et al. (2012) ran 60 mm<sup>2</sup> and 80 mm<sup>2</sup> planar cells for about 500 hours each and were producing around 15 and 60 watts for each size cell, respectively (Figure 18) (Papadam et al., 2012).

Although both groups obtained results that show the potential of SOFCs operating on biogas, button cell research is limited due to the smaller active area of the cell, as well as the lack of a concentration gradient over the length of the cell (*Standardization, n.d.*), causing the results of the button cell research to not be directly applicable to large-scale SOFCs that are used in commercialized SOFC systems.

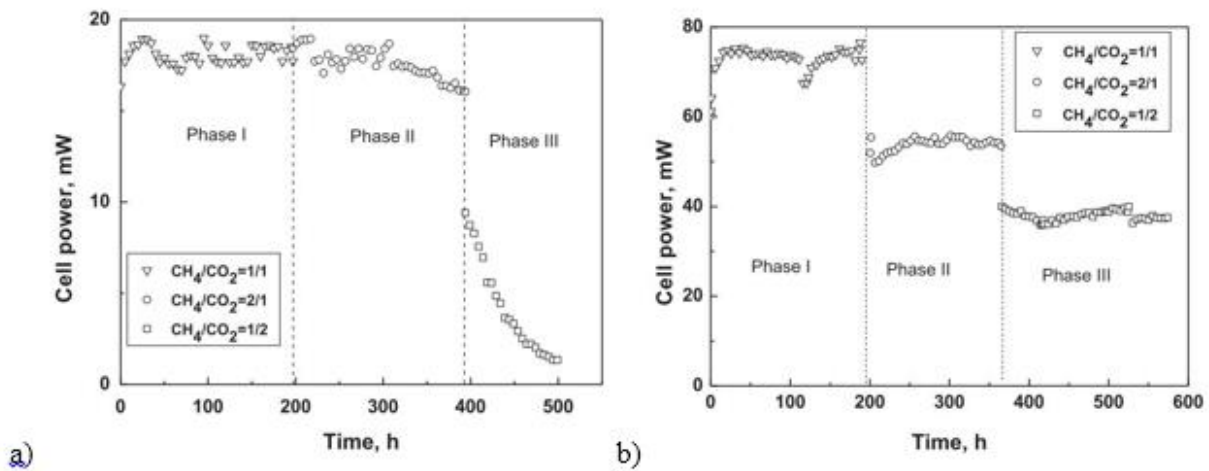


*Figure 18: a) 500 hour test for 60 mm<sup>3</sup> button cell, b) 500 hour test for 80 mm<sup>3</sup> button cell (Papadam et al., 2012).*

The Bloom Energy Server<sup>®</sup> is one of the few large-scale SOFC-biogas systems in the market today. The system runs on natural gas or “directed biogas” and produces about 250 kW of power. Apple has a data center in North Carolina that is currently running on this “Bloom Box,” however, the biogas that the system is said to run on is really just pumped through natural gas pipelines. This means that the system is running on mostly natural gas with small amounts of biogas, not solely on biogas (Fitzsimmons, 2013).

In addition to the Bloom Energy system, there have been a few studies done on theoretical analysis of large-scale biogas-SOFC systems. Mebarki et al. (2015) observed the effects of temperature, electrolyte thickness, and hydrogen concentration on the power density of the

SOFC. The biogas characteristics were calculated based on the biogas production at a landfill in Batna, Algeria. The study assumed an efficiency for the SOFC system of 50%. The optimum temperature, electrolyte thickness, and hydrogen concentration are 1273 K, 0.1 mm, and  $>0.5$ , respectively. Although this theoretical study does consider large-scale systems, there is still a lack of experimental data. In contrast to theoretical studies, experimental studies on large-scale systems allow working through practical problems encountered with the system (Mebarki et al., 2015).



*Figure 19: Bloom Energy Server<sup>®</sup> at Apple's data center (Fehrenbacher, 2013).*

The work performed in this research, therefore, aims to bridge the gap between the reported experimental research on small milliwatt-scale SOFCs fed with biogas, and larger watt-scale reactors that have the potential to be used in a commercially available SOFC system.

### 3. Methodology

A schematic of the testing apparatus used for this study is shown in Figure 20, wherein the tubular SOFC is enclosed on a tubular furnace and connected to various gas cylinders via mass flow controllers as well as a load box and data acquisition system along with a MS for effluent composition analysis.

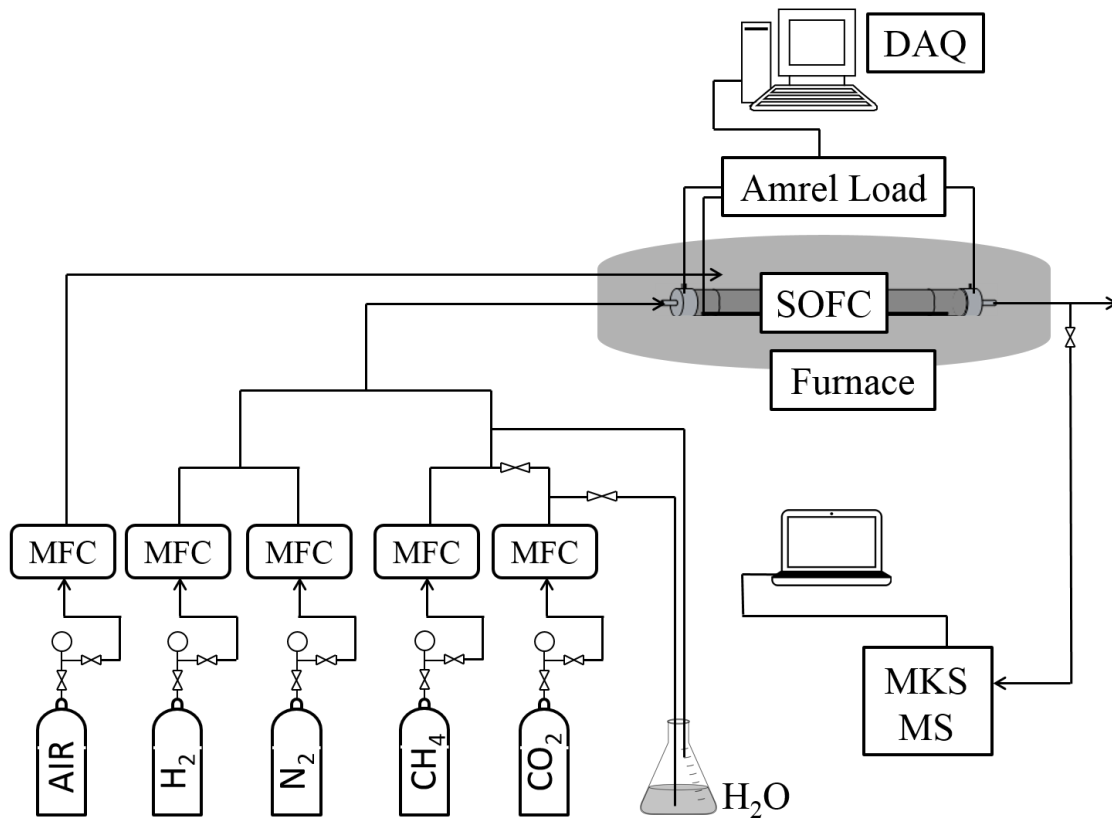


*Figure 20: PFD for the biogas-SOFC system.*

Throughout this study, Protonex's tubular SOFCs were used. The SOFCs had an active area of about 32 cm<sup>2</sup> with a length and diameter of 100mm and 10.2mm, respectively. The cells had a NiYSZ anode (thickness of about 1mm), a ZrO<sub>2</sub> electrolyte (thickness of about 15μm), and a LSCF cathode (thickness of about 30-50μm). The gases for the experiments were obtained from Maine Oxy in the form of high-pressure gas bottles.

The gas flow rate was controlled using Alicat Scientific mass flow controllers (model number: MC-2SLPM-D/5M). Gases were mixed online before entering the fuel cell. For the experiments where the gas was bubbled through water, a 500-mL flask was used as the water container. The flask was sealed with a rubber stopper that had 2 monel tubes through it to allow for the gas to enter and exit. The fuel cell rested in an insulated furnace equipped with K-type Omega Thermocouples (model number: CHAL-020-24) to monitor and control temperature. Through interconnects the SOFC was connected to an American Reliance, Inc. (AMREL) load bank (model number: FEL 60-1) via which the electrical properties could be determined. The set-up of the test stand is shown in Figure 21.

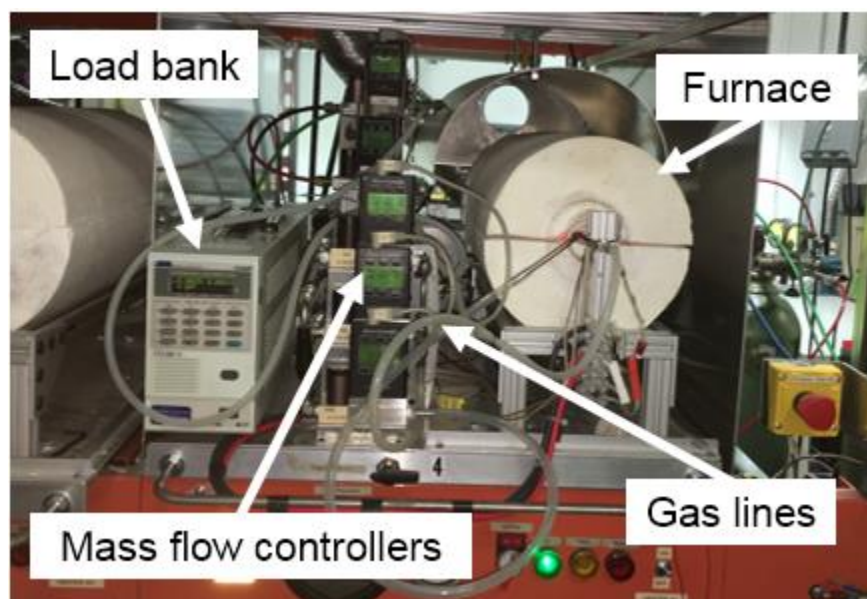


*Figure 21: T-SOFC Test Stand Set-Up.*

The load bank and mass flow controllers were both controlled using a data acquisition software system developed in-house at Protonex. Some of the experiments required the use of mks Spectra Products's Cirrus™ mass spectrometer (MS) (Figure 22).



*Figure 22: mks Spectra Products Mass Spectrometer.*

This MS was used in conjunction with mks's Process Eye Professional software. The MS was calibrated for H<sub>2</sub> and CO.

### **3.1 Effect of Biogas Composition on SOFC Performance**

The first objective of this study was to determine how the composition of biogas affects the performance of the cell. Biogas typically exits a biodigester at 50-75% CH<sub>4</sub>, 25-50% CO<sub>2</sub>, and with trace amounts of H<sub>2</sub>O, N<sub>2</sub>, H<sub>2</sub>, and H<sub>2</sub>S (*Biogas*, n.d.). For this study, the synthetic biogas used consisted of only CH<sub>4</sub> and CO<sub>2</sub>, although some of the experiments included some water vapor as well. The total fuel flow rate was kept constant at 0.2 SLPM, but the ratio of CH<sub>4</sub> flow to CO<sub>2</sub> flow rate was varied to attain a desired feed ratio.

The following CH<sub>4</sub>:CO<sub>2</sub> ratios were studied: 40:60, 45:55, 50:50, 55:45, and 60:40. The 60:40 CH<sub>4</sub>:CO<sub>2</sub> composition only ran for 45 minutes before breaking due to coke build-up, so even though typical biogas composition is in that range, testing for this study was 40:60 – 55:45 CH<sub>4</sub>:CO<sub>2</sub> ratio range. Work is currently being done on the effects of adding oxygen and steam to

a more typical simulated biogas composition (60:40 CH<sub>4</sub>:CO<sub>2</sub>) to drive down the methane composition entering the cell, and maintain a high lifetime.

For this objective, the fuel utilization, i.e., the ratio of actual current applied to maximum possible current density based on the amount of fuel, was maintained at a modest 50% to prevent any issues due to a fuel utilization that was either too high or too low. For this objective, the fuel utilization was calculated simply by determining the maximum current that would result if all of the methane were converted to hydrogen, and taking 50% of that value. This calculation was suitable for this experiment, but a more accurate calculation based on equilibrium conversion of the reactants was used and described with Objective 2.

Once the SOFC was placed in the furnace, the cell was heated to 900°C with hydrogen flowing through the cell. A temperature of 900°C was chosen due to the desire to maximize conversion of CH<sub>4</sub>, and thus, minimize coking, as described in section 2.3.1. The temperature of the cell was maintained at 900°C for 3 hours to reduce the nickel (II) oxide on the anode to nickel under the hydrogen atmosphere. Once the reducing procedure was complete, the cell ran under constant current density for 1 hour so that a comparison could be made between the biogas results and the hydrogen. Following the constant current density, polarization plot data was obtained for the cell under hydrogen conditions. After the polarization plot, the inlet fuel transitioned from hydrogen to simulated biogas. To allow for the cell to remain at 900°C, the hydrogen was not shut off until the methane and carbon dioxide were flowing through the cell. Once the hydrogen was off, a polarization plot was obtained under biogas conditions, and then the constant current density conditions were set and the fuel cell run under these conditions for 150 hours to determine stability and durability. The shut-down procedure involved cooling the cell while hydrogen flowed through the cell. This procedure was used for each of the 5 CH<sub>4</sub>:CO<sub>2</sub> ratios studied in this

experiment. Figure 23 shows a screenshot of part of the data acquisition software procedure written for this experiment.

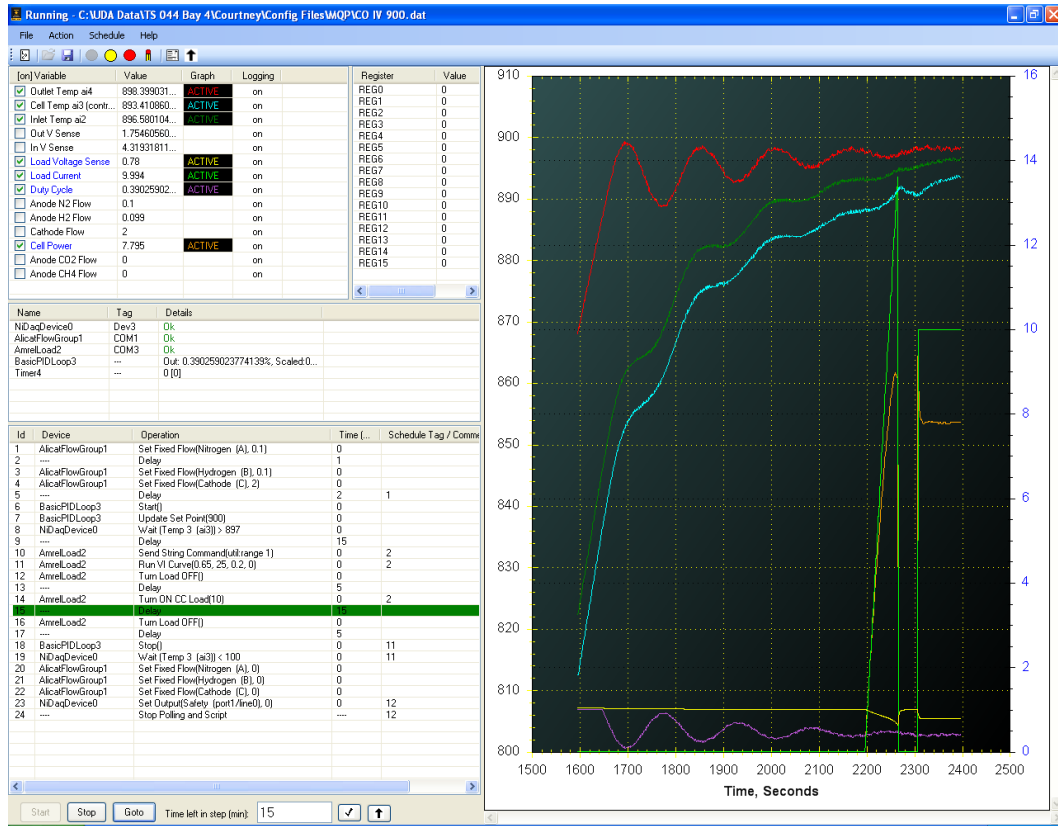


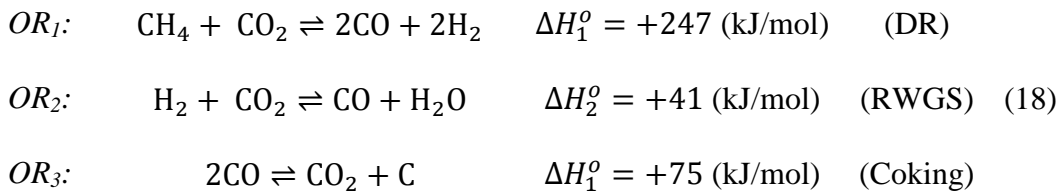
Figure 23: Universal Data Acquisition (UDA) Software Interface.

### 3.2 Effect of Fuel Utilization on SOFC Lifetime

The second objective was to determine how fuel utilization affected the performance of the cell. The results of Objective 1 suggested that of the 5 CH<sub>4</sub>:CO<sub>2</sub> ratios, a 45:55 CH<sub>4</sub>:CO<sub>2</sub> mixture had the longest lifetime. Because of this finding, the 45:55 CH<sub>4</sub>:CO<sub>2</sub> mixture was kept constant throughout all experiments conducted under Objective 2.

Five different fuel utilization values were studied for this objective. The current densities required to achieve the desired fuel utilization values were calculated using the equilibrium constant of the reaction at 900°C.

Due to the presence of Ni catalyst and the high operating temperature (900 °C), we can assume that there is gas-phase reaction equilibrium in effect among the gas-phase species at the tube exit. There are  $n = 6$  species (CH<sub>4</sub>, CO<sub>2</sub>, CO, H<sub>2</sub>, H<sub>2</sub>O, and C), and  $e = 3$  elements. Thus, the number of independent overall reactions (ORs) needed for a thermodynamic or kinetic analysis is  $\mu = n - e = 3$ . Any set of 3 independent ORs would suffice for this purpose. Therefore, we may pick the following set:



From the standard thermodynamic data for these species at 298 K:

| <i>Species</i>   | $H_{i,298}^{\circ}$ (kJ/mol) | $S_{i,298}^{\circ}$ (J/molK) | $G_{i,298}^{\circ}$ (kJ/mol) |
|------------------|------------------------------|------------------------------|------------------------------|
| CH <sub>4</sub>  | -74.852                      | 186.27                       | -50.836                      |
| H <sub>2</sub> O | -241.818                     | 188.72                       | -228.589                     |
| CO <sub>2</sub>  | -393.505                     | 213.67                       | -394.384                     |
| CO               | -110.541                     | 197.90                       | -137.277                     |
| H <sub>2</sub>   | 0                            | 130.59                       | 0                            |
| C                | 0                            | 5.694                        | 0                            |
| O <sub>2</sub>   | 0                            | 205.00                       | 0                            |

(19)

Further assuming the species entropy and enthalpy of formation to be constant with temperature and using  $\Delta G_{OR}^{\circ} = \Delta H_{OR}^{\circ} - T\Delta S_{OR}^{\circ}$ , the standard Gibbs free energy of the above three ORs may

be plotted as a function of temperature to determine their operating temperatures of feasibility, i.e., when the  $\Delta G_{OR}^{\circ} < 0$ . An example of such a plot is provided (Figure 24).

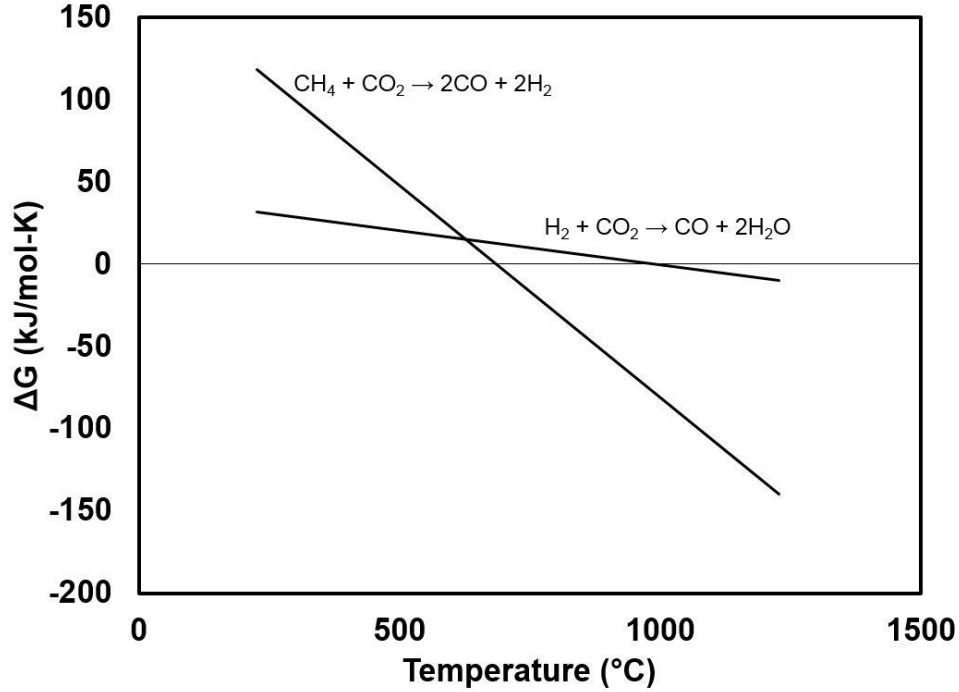


Figure 24: Gibbs free energy for the DR and RWGS reactions.

Further, from

$$K_{OR} = \exp\left(-\frac{\Delta G_{OR}^{\circ}}{RT}\right) = \exp\left(-\frac{\Delta S_{OR}^{\circ}}{RT}\right) \exp\left(-\frac{\Delta H_{OR}^{\circ}}{RT}\right) \quad (20)$$

we can write

$$K_{OR} = K_{OR,298} \exp\left\{-\frac{\Delta H_{OR}^{\circ}}{RT} \left(\frac{1}{T} - \frac{1}{298}\right)\right\} \quad (21)$$

for the above three equations and writing these in terms of  $\chi_1$ ,  $\chi_2$ , and  $\chi_3$ , the equilibrium conversions for the three ORs, the feed gas ratio, and the current drawn, one can solve for these three independent nonlinear equations via root finding (e.g., Newton's method, using Maple or Mathematica, etc.). This would correspond to the exit conditions in the absence of current

assuming reaction equilibrium is attained inside the SOFC tube, so that the exit gas composition can be determined.

If C is neglected, only 2 equations are needed. Let us analyze this case first, as at any rate the amount converted to C is small. Then from the above data for the DRR

$$\begin{aligned}\Delta H_{A1}^o &= +247.275 \text{ kJ/mol} \\ \Delta S_{A1}^o &= +257.04 \text{ J/mol-K} \\ \Delta G_{A1}^o &= +170.669 \text{ kJ/mol}\end{aligned}\tag{22}$$

where A in the subscript refers to anode, and 1 alludes to OR<sub>1</sub>. In other words, the reaction is highly endothermic and endergonic at room temperature, with the reaction equilibrium constant being virtually zero for the DR reaction. Actually,

$K_{A1,298} = \exp\left(-\frac{\Delta G_{A1,298}^o}{RT}\right) = 1.25 \times 10^{-30}$ . However, at 900°C, the reaction becomes quite exergonic owing to the change in Gibbs free energy with temperature, and  $K_{A1,1173} = 257.75$ .

Similarly for the RWGSR, the standard Gibbs free energy and enthalpy of the reaction are given by

$$\begin{aligned}\Delta H_{A2}^o &= +41.146 \text{ kJ/mol} \\ \Delta S_{A2}^o &= +42.36 \text{ J/mol-K} \\ \Delta G_{A2}^o &= +28.518 \text{ kJ/mol}\end{aligned}\tag{23}$$

In other words, the reaction is endothermic and endergonic at room temperature, with the reaction equilibrium constant being  $K_{A2,298} = \exp\left(-\frac{\Delta G_{A2,298}^o}{RT}\right) = 1.0 \times 10^{-5}$ . However, at 900°C, the reaction becomes exergonic, and  $K_{A2,1173} = 2.40$ .

With the equilibrium constants being determined at 900°C, the extents of the two reactions can next be determined, from which the equilibrium gas composition can be determined as follows.

Recall that the molar flow rate  $\dot{n}_i$  of a species  $i$  in a flow reactor is related to the  $q$  independent reaction extents  $\dot{\xi}_\rho \equiv \int^V r_\rho dV$  as follows (Fogler, 4<sup>th</sup> ed.)

$$\dot{n}_i = \dot{n}_{i,0} + \sum_{\rho=1}^q \nu_{\rho i} \dot{\xi}_\rho \quad (i = 1, 2, \dots, n) \quad (24)$$

Summing these over all species, the total molar flow rate

$$\dot{n}_T = \dot{n}_{T,0} \left( 1 + \chi_{A0} \sum_{\rho=1}^q \Delta \nu_\rho \chi_\rho \right) \quad (25)$$

where  $\chi_{A0}$  is the feed mole fraction of the key reactant A (CH<sub>4</sub>), and the change in the number of moles in reaction  $\rho$ ,  $\Delta \nu_\rho$ , and the dimensionless reaction extent  $\chi_\rho$  are defined by the following

$$\dot{\nu}_\rho = \sum_{i=1}^n \nu_{\rho i} \quad \chi_\rho \equiv \frac{\dot{\xi}_\rho}{\dot{n}_{A,0}} \quad (\rho = 1, 2, \dots, n) \quad (26)$$

where  $\dot{n}_{A,0}$  is the feed molar flow rate of the key reactant A (CH<sub>4</sub>).

Finally, the mole fraction of the species,  $x_i = \frac{\dot{n}_i}{\dot{n}_T}$

$$x_i = \frac{\theta_i + \sum_{\rho=1}^q \nu_{\rho i} \chi_\rho}{\frac{1}{x_{A0}} + \sum_{\rho=1}^q \Delta \nu_\rho \chi_\rho} \quad (i = 1, 2, \dots, n) \quad (27)$$

where the molar feed ratio of species  $i$ ,  $\theta \equiv \frac{\dot{n}_{i,0}}{\dot{n}_{A,0}}$ .

This provides the following mole fractions for the five species participating in the two non-electrocatalytic electrode reactions, namely the DRR and the RWGSR. Here  $\Delta v_{DRR} = +2$ , and  $\Delta v_{RWGS} = 0$ , i.e., there is no change in the number of moles in the RWGSR.

$$\begin{aligned}
 x_{\text{CH}_4} &= \frac{1 + (-1)\chi_1}{\frac{1}{\chi_{\text{CH}_4}} + 2\chi_1} & x_{\text{CO}_2} &= \frac{\theta_{\text{CO}_2} + (-1)\chi_1 + (-1)\chi_2}{\frac{1}{\chi_{\text{CH}_4,0}} + 2\chi_1} \\
 x_{\text{H}_2\text{O}} &= \frac{\theta_{\text{H}_2\text{O}} + (0)\chi_1 + (+1)\chi_2}{\frac{1}{\chi_{\text{CH}_4,0}} + 2\chi_1} & x_{\text{H}_2} &= \frac{\theta_{\text{H}_2} + (+2)\chi_1 + (-1)\chi_2}{\frac{1}{\chi_{\text{CH}_4,0}} + 2\chi_1} \\
 x_{\text{CO}} &= \frac{\theta_{\text{CO}} + (+2)\chi_1 + (+1)\chi_2}{\frac{1}{\chi_{\text{CH}_4,0}} + 2\chi_1}
 \end{aligned} \tag{28}$$

These are substituted into the equilibrium constant mass action relations for the two reactions, i.e.,

$$K_{A1} = \frac{x_{\text{CO},e}^2 x_{\text{H}_2,e}^2}{x_{\text{CH}_4,e} x_{\text{CO}_2,e}} \quad K_{A2} = \frac{x_{\text{CO},e} x_{\text{H}_2\text{O},e}}{x_{\text{CH}_4,e} x_{\text{CO}_2,e}} \tag{29}$$

which may be solved simultaneously numerically via rootfinding (e.g., using Mathematica or Polymath) to find the two equilibrium dimensionless extents  $\chi_{1,e}$  and  $\chi_{2,e}$ .

As an example, for the feed ratio,  $\text{CH}_4:\text{CO}_2 = 45:55$  and no water in the feed,  $\theta_{\text{CO}_2} = 55/45$ ,  $\theta_{\text{H}_2\text{O}} = \theta_{\text{H}_2} = \theta_{\text{CO}} = 0$  and  $x_{\text{CH}_4,0} = 0.45$ , rootfinding provides the two equilibrium dimensionless extents  $\chi_{1,e} = 0.9643$  and  $\chi_{2,e} = 0.1722$ . When these are substituted into the above relationships, the calculated equilibrium mole fractions are:

$$x_{\text{CH}_4,e} = 0.0086; x_{\text{CO}_2,e} = 0.0207; x_{\text{H}_2\text{O},e} = 0.0415; x_{\text{H}_2,e} = 0.4231; x_{\text{CO},e} = 0.5061.$$

For this system, current is generated through the oxidation of both H<sub>2</sub> and CO. For this objective, it was assumed that 100% fuel utilization meant that all of the available H<sub>2</sub> and CO were oxidized to form H<sub>2</sub>O and CO<sub>2</sub>. The experiments performed for Objective 5 determine the actual ratio of current produced from H<sub>2</sub> versus CO.

Equation 30 was used to calculate the current generated from the oxidation of all the H<sub>2</sub> produced at equilibrium, and Equation 31 was used to calculate the current generated from the oxidation of all the CO produced at equilibrium. The mole flow ( $\dot{n}_{H_2}$ ) was calculated using the ideal gas law ( $\dot{n}_i = \frac{PV}{RT}$ ) where pressure was considered atmospheric, 1 atm, and the for the case of hydrogen, volumetric flow rate was calculated by multiplying the hydrogen composition,  $x_{H_2}$ , by the total volumetric flow rate, 0.2 SLPM.

$$I_{100\%,H_2} = \frac{\dot{n}_{H_2}}{60 \text{ sec}} \times 2 \text{ mol } e^- \times F \quad (30)$$

$$I_{100\%,CO} = \frac{\dot{n}_{CO}}{60 \text{ sec}} \times 2 \text{ mol } e^- \times F \quad (31)$$

The current at the desired fuel utilization,  $I_{U_f}$ , was calculated using equation 32 .

$$I_{U_f} = U_f \times (I_{100\%,H_2} + I_{100\%,CO}) \quad (32)$$

Fuel utilization values of 36%, 50%, 63%, 76%, and 92% were chosen for study for this objective. The respective current values are as follows: 7.24 A, 10.33 A, 12.92 A, 15.51 A, and 18.81 A. The reducing procedure and the constant current procedure described in Objective 1 were used for each fuel utilization condition tested in this objective, however, for the fuel utilization experiments, the cells ran under constant current density for 250 hours each instead of 150 hours, as done for experiments in 3.1.

### **3.3 Effect of Moisture in Feed on Cell Lifetime**

The third objective of the study was to determine if adding water to the synthetic biogas mixture improved the performance and/or lifetime of the cell. It was predicted that the increased partial pressure of water would improve the cell performance due to a potential increase in steam reforming of methane coupled with coke cleansing. The water was added to the mixture by bubbling the CO<sub>2</sub> through a 2-L flask filled about half way with water at room temperature.

The humidified CO<sub>2</sub> was then mixed with the CH<sub>4</sub> and the CO<sub>2</sub>-CH<sub>4</sub>-H<sub>2</sub>O mixture entered the cell. To determine the composition of water in the mixture, the flask was weighed before and after each run and the difference between those measurements was assumed to be the amount of water that entered the cell over the amount of time recorded. The approximate composition for all runs was 3 wt.% water. Another way to determine the composition of the water is by knowing that the vapor pressure of water at room temperature should be equal to the composition of the water in the gas stream. The vapor pressure of water at room temperature is about 0.03 atm., which confirms that the composition of water in the gas stream is about 3 wt.%.

The cell underwent the same procedure as described in Objective 1, where data was collected to generate a polarization plot before and after running the cell for 250 hours at constant current density. Two cells were run for this experiment, one operated at 50% fuel utilization and the other operated at 76% fuel utilization.

### **3.4 Mass Spectrometry Analysis on the Outlet Gas of the Single-Cell SOFC**

A mass spectrometer analysis of the effluent gas composition was needed in order to determine the extent of the reactions occurring in the cell, as well as the ratio of the oxidation rate of H<sub>2</sub> to

the oxidation rate of CO. This ratio was used to determine the actual values of the fuel utilization.

The inlet capillary tube of the MS was fed through the outlet end of the fuel cell as shown in Figure 25.



*Figure 25: MS capillary in the outlet end of the fuel cell.*

The fuel cell exit gas was passed through the MS and the partial pressure of each species was recorded within mks's Process Eye Professional software. The raw values recorded did not consider the ionization probability of each species, so all of the partial pressure values were further divided by their respective ionization probabilities as shown in Appendix A. After this calculation, the mole fraction of the species was able to be calculated based on the new scaled total pressure. To verify the calibration of the MS data thus acquired, a calibration curve was generated by feeding a series of CO/H<sub>2</sub> blends at known concentrations through the MS. All the data obtained in this objective was fit to this calibration curve (Figure 26).

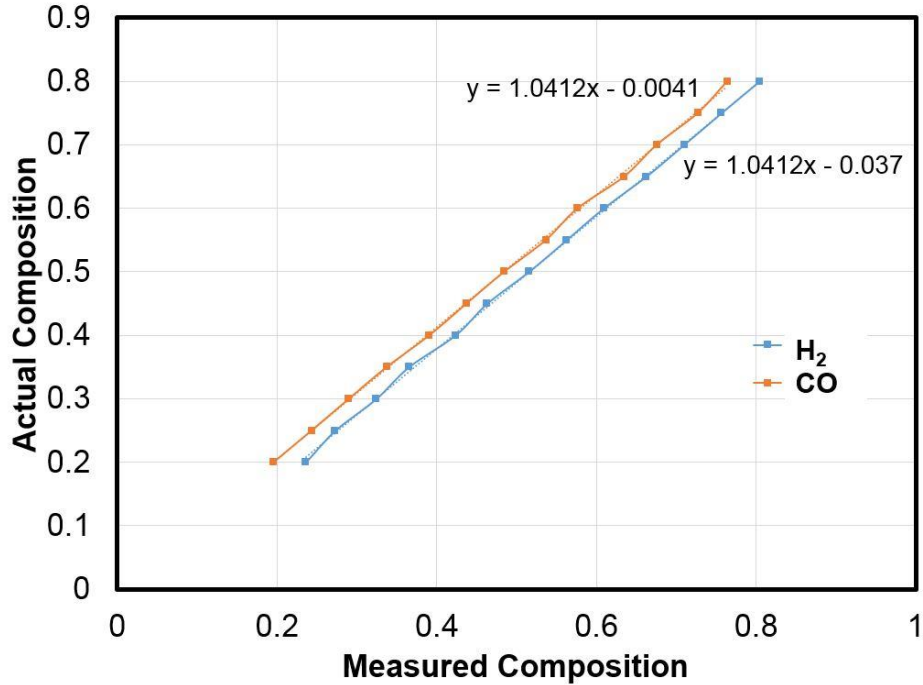


*Figure 26: H<sub>2</sub> and CO MS calibration curve.*

The MS was operated while a cell was running on 45:55 CH<sub>4</sub>:CO<sub>2</sub> at OCV at 900°C in order to determine the extent of the DR and RWGS reactions (Equation 15). The cell was reduced under hydrogen conditions as explained in section 3.1, and then converted over to the CH<sub>4</sub> and CO<sub>2</sub> blend. The cell was held at OCV under these conditions for 30 minutes to obtain steady data for the equilibrium concentrations of the species.

As the current increased, the H<sub>2</sub> and CO were both oxidized to form H<sub>2</sub>O and CO<sub>2</sub>. To examine the relationship between the species during oxidation, the MS was used to measure the composition of each species at incremental current values. The cell load was held constant for 5 minutes at each current value to ensure equilibrium. The mole fractions of the species were plotted against current to observe the reactions occurring during oxidation.

### 3.4 Effects of 45:55 CH<sub>4</sub>:CO<sub>2</sub> Fuel Through a 5-Cell SOFC Assembly

In addition to the single-cell testing, one test bay was retrofitted to run a pre-made 5-cell T-SOFC assembly (Figure 27).



*Figure 27: 5-Cell T-SOFC Assembly.*

With a 5-cell stack, the total fuel flow rate through the cell was 1 SLPM. This flow rate was consistent with the single-cell flow rate ( $0.2 \text{ SLPM} \times 5 \text{ cells} = 1 \text{ SLPM}$ ). To maintain the 45:55 CH<sub>4</sub>:CO<sub>2</sub> ratio with a total flow rate of 1 SLPM, the flow rates of CH<sub>4</sub> and CO<sub>2</sub> were 0.45 SLPM and 0.55 SLPM, respectively. The reducing procedure for the cells was similar to that for the single-cell test (section 2.1), however, the cells were reduced at 700°C instead of 900°C to prevent the interconnects from melting while reducing the cells at OCV for 3 hours. Following the reduction, a polarization plot was generated for the stack running under hydrogen. After that, the temperature was brought up to 900°C and the fuel was changed from hydrogen to the 45:55 CH<sub>4</sub>:CO<sub>2</sub> mixture. Shortly after, a polarization plot was generated for the stack running on the

synthetic biogas mixture, and then, to obtain lifetime information for the stack, it was allowed to run for as long as it could before breaking, which turned out to be about 35 hours.

## 4. Results and Discussion

### 4.1 Effect of Biogas Composition on SOFC Performance

The first objective was to determine how the composition of biogas affects the performance of the SOFC. Five different  $\text{CH}_4:\text{CO}_2$  ratios were tested in addition to pure  $\text{H}_2$  and  $\text{CO}$ . Figure 28 shows polarization curves for  $\text{H}_2$  and  $\text{CO}$  at  $900^\circ\text{C}$ . Figure 29 shows polarization curves for all five biogas ratios, and for pure  $\text{H}_2$  and  $\text{CO}$  all at  $900^\circ\text{C}$ . For the experiments with biogas, the total fuel flow ( $\text{CO}_2$  and  $\text{CH}_4$ ) through the cell was 0.2 SLPM with air flowing over the cathode at 2 SLPM. For the experiment with  $\text{H}_2$  and  $\text{CO}$ , the fuel flow was set at 0.2 SLPM with air flowing over the cathode at 2 SLPM.

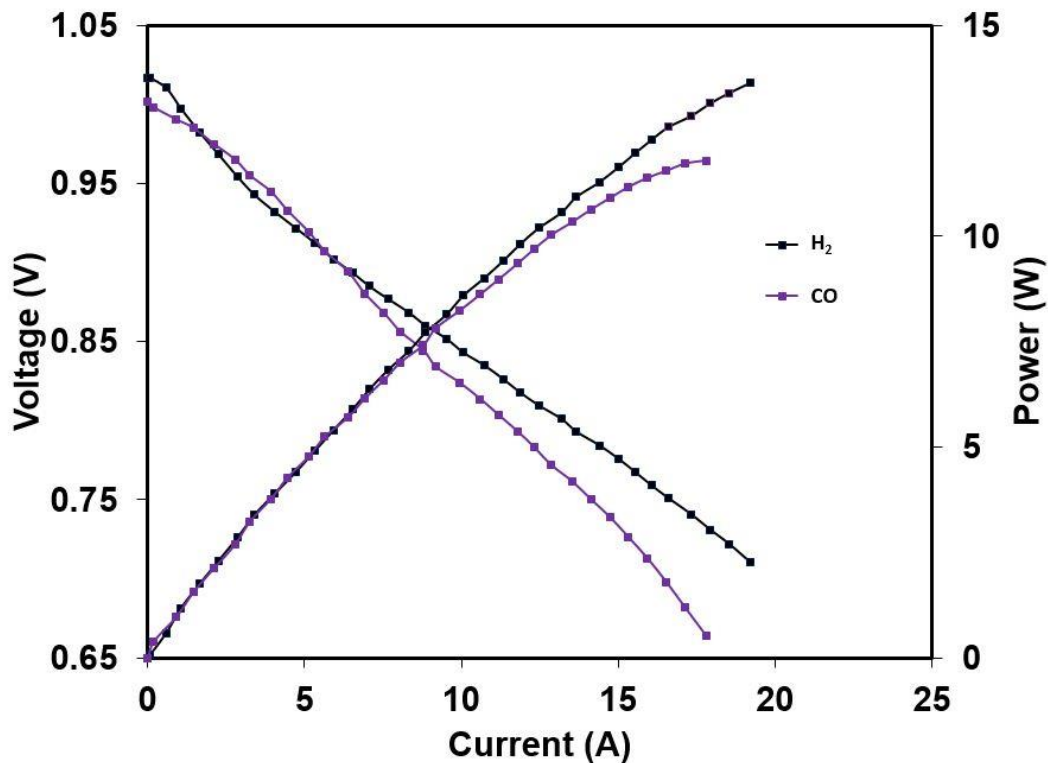
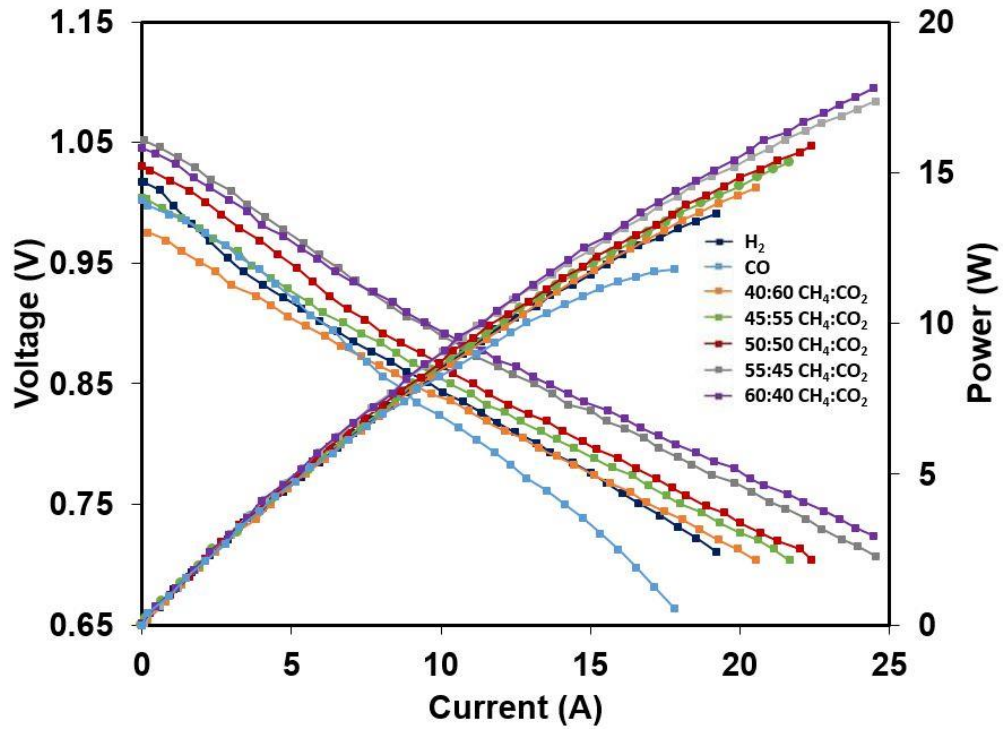
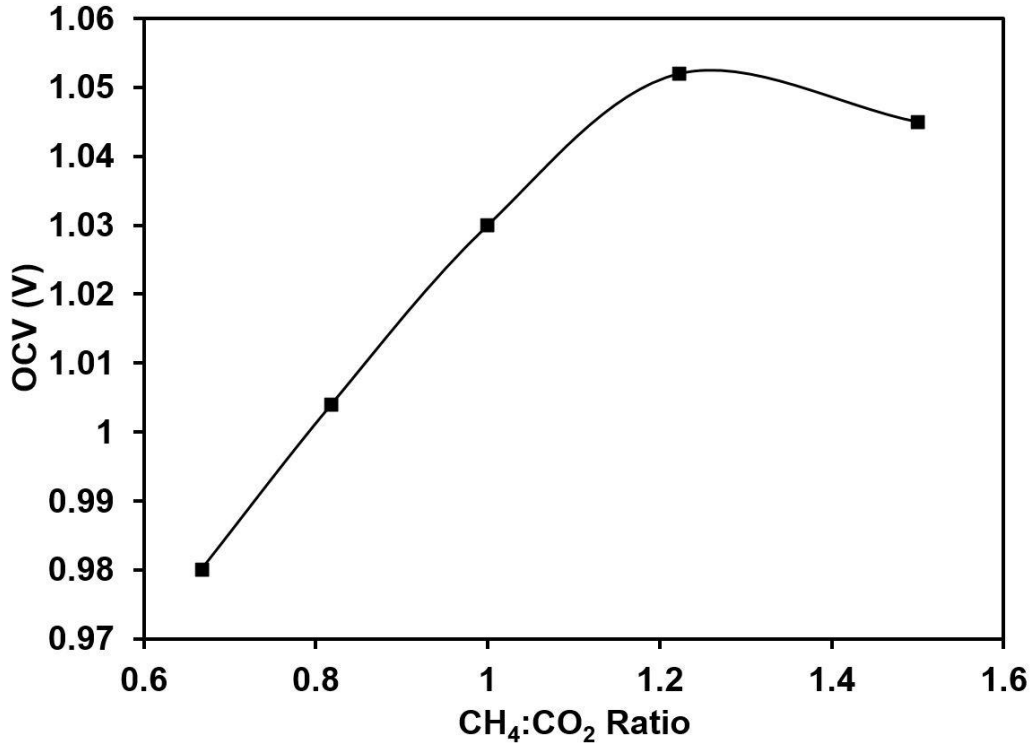


Figure 28: Polarization curve for  $\text{H}_2$  and  $\text{CO}$  at  $900^\circ\text{C}$ .



*Figure 28: Polarization curves for 5 CH<sub>4</sub>:CO<sub>2</sub> ratios and pure H<sub>2</sub> and CO.*

According to Figure 29 there is a trend in the open circuit voltage (OCV) with respect to CH<sub>4</sub>:CO<sub>2</sub> ratio. In general, the greater CH<sub>4</sub>:CO<sub>2</sub> ratio, the greater the OCV (shown in Figure 30).



*Figure 29: OCV Values for various CH<sub>4</sub>:CO<sub>2</sub> ratios.*

The lifetime of a cell running on each CH<sub>4</sub>:CO<sub>2</sub> ratio was tested by drawing constant current density for 150 hours for each test (Figure 31). As predicted by the thermodynamic and Gibbs free energy calculations, steady state operation at 700°C was not feasible due to short lifetime (~20 minutes) (Figure 30). For this experiment at 700°C, voltage was held constant at 0.7 V and the composition entering the cell was similar to that of actual biogas at 60:40 CH<sub>4</sub>:CO<sub>2</sub>.

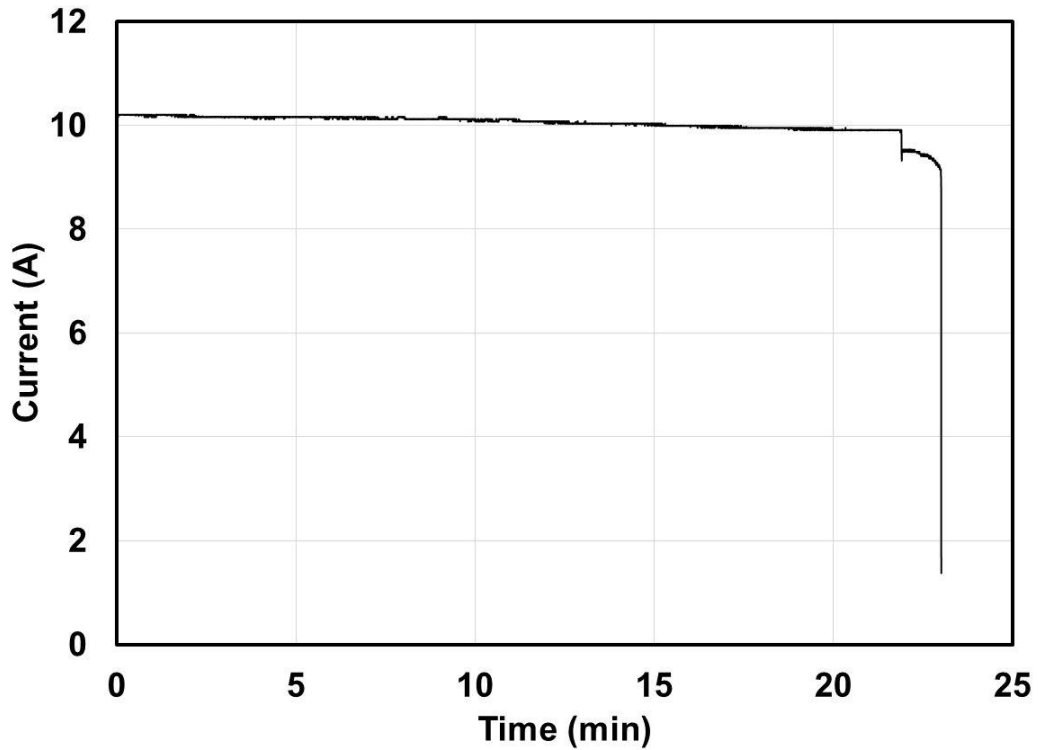


*Figure 30: Lifetime plot for 60:40 CH<sub>4</sub>:CO<sub>2</sub> at 700°C and 0.7 V.*

As expected based on the polarization curve, the greater CH<sub>4</sub>:CO<sub>2</sub> ratio, the greater the initial power density, however, the rates of degradation for 55:45 and 50:50 CH<sub>4</sub>:CO<sub>2</sub> ratios were greater than those for the 45:55 and 40:60 CH<sub>4</sub>:CO<sub>2</sub> ratios. Table 3 shows the degradation slopes for each composition as well as the amount of time it would take for each cell to degrade by 10%.

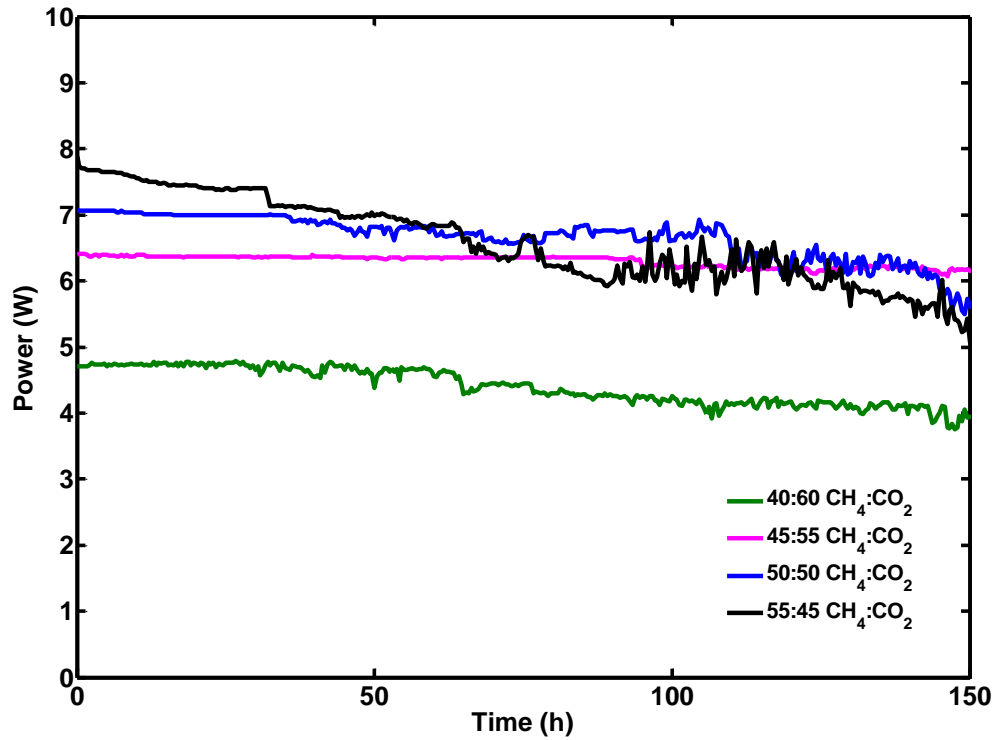


Figure 31: Lifetime plots for 4  $\text{CH}_4:\text{CO}_2$  ratios.

Table 3: Lifetime data for 4  $\text{CH}_4:\text{CO}_2$  ratios.

| $\text{CH}_4:\text{CO}_2$ Ratio | Slope   | 10% Lifetime (h) |
|---------------------------------|---------|------------------|
| 40:60                           | -0.0061 | 79               |
| 45:55                           | -0.0012 | 4797             |
| 50:50                           | -0.0069 | 103              |
| 55:45                           | -0.015  | 51               |

As shown by the noise in Figure 31, the performance of the 50:50 and 55:45  $\text{CH}_4:\text{CO}_2$  ratios was poor after about 30 hours, but the initial power was the highest for the 50:50 and 55:45  $\text{CH}_4:\text{CO}_2$  ratios. The 45:55  $\text{CH}_4:\text{CO}_2$  ratio shows more stable operation than the higher ratios, but the initial power is lower. Somewhat unexpectedly, the 40:60  $\text{CH}_4:\text{CO}_2$  ratio also shows a steep degradation slope, and a fair amount of noise after about 40 hours of operation.

Table 3 shows the degradation slopes of each ratio, as well as the amount of time before the cell would degrade by 10%, a number indicative of the point at which there would be operational difficulties with a system. Although the 45:55 CH<sub>4</sub>:CO<sub>2</sub> ratio did not produce the highest power, it had the smallest degradation slope, and thus, the longest 10% lifetime at almost 5,000 hours. Despite the high power produced with the 55:45 CH<sub>4</sub>:CO<sub>2</sub> ratio, this ratio showed the largest degradation slope, and thus the shortest 10% lifetime at only 50 hours.

As shown in Figure 29, the performance of pure H<sub>2</sub> was better than the performance of pure CO at 900°C. At the higher CH<sub>4</sub>:CO<sub>2</sub> ratios there is excess CH<sub>4</sub> that has not been converted via the dry reforming reaction, and at lower CH<sub>4</sub>:CO<sub>2</sub> ratios there is excess CO that has not been converted. When there is excess CH<sub>4</sub>, the CH<sub>4</sub> undergoes pyrolysis producing carbon and additional H<sub>2</sub>



As explained in section 2.3.1, carbon is detrimental to the performance of the cell. The additional H<sub>2</sub> produced from in this reaction could partly explain the high initial power and short-term performance of the higher CH<sub>4</sub>:CO<sub>2</sub> ratios, but the carbon produced in the reaction could be the cause of the short lifetime of the higher CH<sub>4</sub>:CO<sub>2</sub> ratios.

The 40:60 CH<sub>4</sub>:CO<sub>2</sub> ratio has excess CO<sub>2</sub>, which is likely to produce CO via the water gas shift reaction



According to Figure 29, pure CO does not perform as well as pure H<sub>2</sub>. Because the CO does not perform as well as H<sub>2</sub>, the initial power value for the lower CH<sub>4</sub>:CO<sub>2</sub> ratio (excess CO<sub>2</sub> that forms CO) was lower than those for higher CH<sub>4</sub>:CO<sub>2</sub> ratios (excess CH<sub>4</sub> that forms H<sub>2</sub>). In

addition, when the CO forms from CO<sub>2</sub>, there is no carbon formation unlike when CH<sub>4</sub> decomposes into carbon and H<sub>2</sub>. The lack of carbon formation causes a longer lifetime for lower CH<sub>4</sub>:CO<sub>2</sub> ratios compared to higher CH<sub>4</sub>:CO<sub>2</sub> ratios as shown in Figure 31 and Table 3.

When the CH<sub>4</sub>:CO<sub>2</sub> ratio is almost 1 as with the 45:55 CH<sub>4</sub>:CO<sub>2</sub> ratio, the conversion of both species via the dry reforming reaction is almost maximized. Unlike the stoichiometric 50:50 CH<sub>4</sub>:CO<sub>2</sub> ratio, the 45:55 CH<sub>4</sub>:CO<sub>2</sub> ratio was superior in ensuring that there was little unconverted methane left to form coke, as discussed in the thermodynamic analysis discussion in Chapter 3. Further, it allows some room for mass flow controller calibration error or incomplete mixing between the species because with the 50:50 CH<sub>4</sub>:CO<sub>2</sub> ratio, any slight excess methane would result in carbon deposition. On the other hand, slight excess CO<sub>2</sub> only reduces power and does not cause any detrimental coking in the cell.

Typically, biogas that exits a biodigester is not a 50:50 CH<sub>4</sub>:CO<sub>2</sub> mixture, but rather a 60:40 CH<sub>4</sub>:CO<sub>2</sub> mixture. Future research aims to test the effects of adding oxygen and water vapor to a more typical simulated biogas composition (60:40 CH<sub>4</sub>:CO<sub>2</sub>) to reduce the methane composition entering the cell down toward the desirable 45:55 CH<sub>4</sub>:CO<sub>2</sub> and maintain the higher lifetime.

## **4.2 Effect of Fuel Utilization on SOFC Lifetime**

The second objective was to determine the effect of fuel utilization on the lifetime of the cells. When varying fuel utilization, the 45:55 CH<sub>4</sub>:CO<sub>2</sub> feed ratio was held constant due to its high lifetime as explained in 4.1. The fuel utilization was set at 35%, 50%, 63%, 76% and 92% for 5 different cells and each cell was run for 250 hours, unless cell failure occurred earlier. Figure 32 shows how the lifetime of a cell running at each fuel utilization was affected by time.

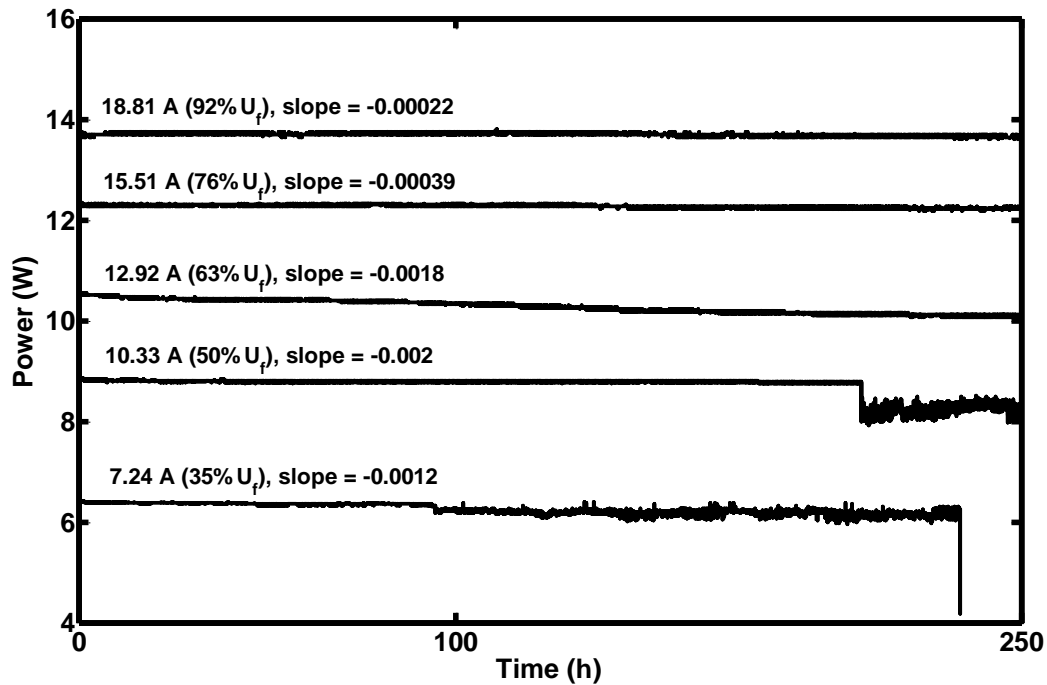


*Figure 32: Lifetime plots for five different fuel utilizations.*

The 35% and 50% utilization curves show noise beginning around 100 hrs and 200 hours, respectively. Although the exact cause of this noise is unknown, it is predicted that this noise originates from the presence of coke on the anode, causing inconsistencies with electron transfer and cracks in the electrolyte. The 63%, 76%, and 92% fuel utilization curves are much more stable, indicating a lack of coke formation under those conditions. Under the hypothesis that coke results primarily from any unconverted methane, it could be rationalized that lower utilization means more unconverted methane leading to more coking and shorter lifetimes. It is also conceivable that at higher fuel utilizations, there is a higher partial pressure of water in the reactor, which helps to flush out any coke there is out of the reactor by reacting with the carbon



The cell running at 76% utilization demonstrated a minimal rate of degradation. Figure 33 shows the polarization plot for the cell running at 76% fuel utilization before and after the cell ran for 250 hours.

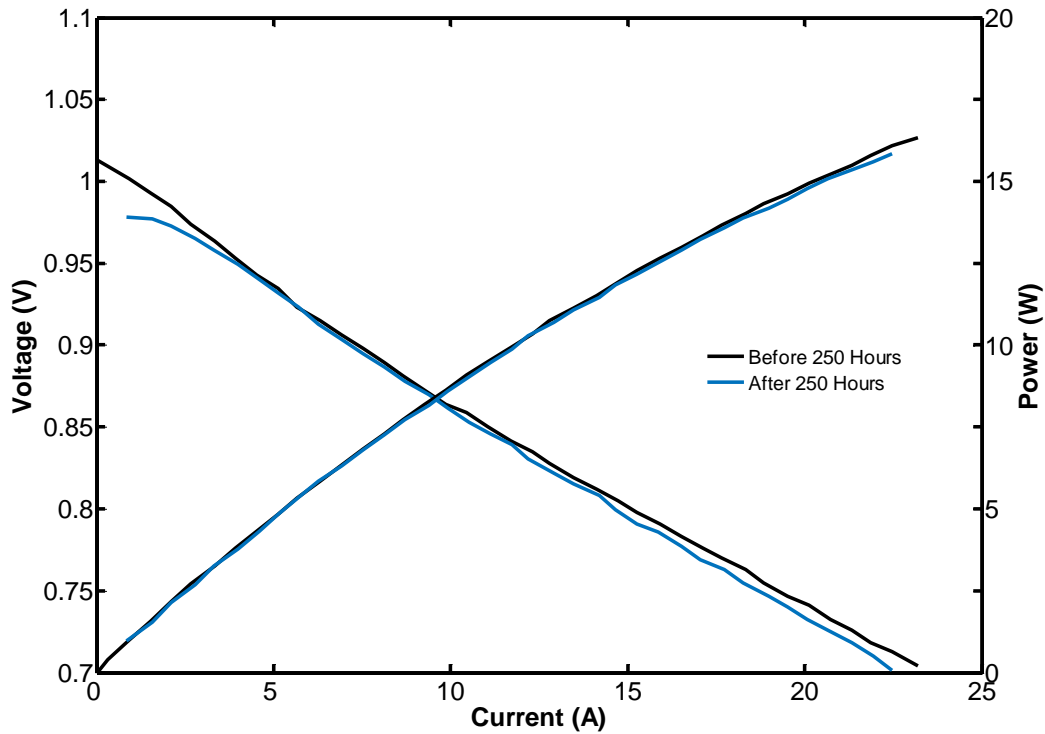


*Figure 33: Polarization curve for before and after 250 hours of operation at 76% fuel utilization.*

Clearly, there is minimal difference between the two plots, indicating that there was no significant amount of coking occurring in the cell running at 76% fuel utilization and a 45:55 CH<sub>4</sub>:CO<sub>2</sub> ratio for 250 hours. Thus, higher utilizations are desirable to extend the life of the fuel cell.

### **4.3 Effect of Moisture in Feed on Cell Lifetime**

The third objective was to determine the effects of water addition in the feed on the lifetime of the cells. To determine if a humidified feed improved the lifetime of the cell, 4 cells were run for

250 hours at a constant current density and with the 45:55 CH<sub>4</sub>:CO<sub>2</sub> ratio. Two of the cells ran at 15.51 A, which corresponded to 76%  $U_f$  humidified and unhumidified, and the other two cells ran at 10.33 A (50%  $U_f$ ) humidified and unhumidified. As shown in Figure 34, the water addition had no effect on the degradation rate of the higher fuel utilization run, but did improve the degradation rate of the lower utilization run.

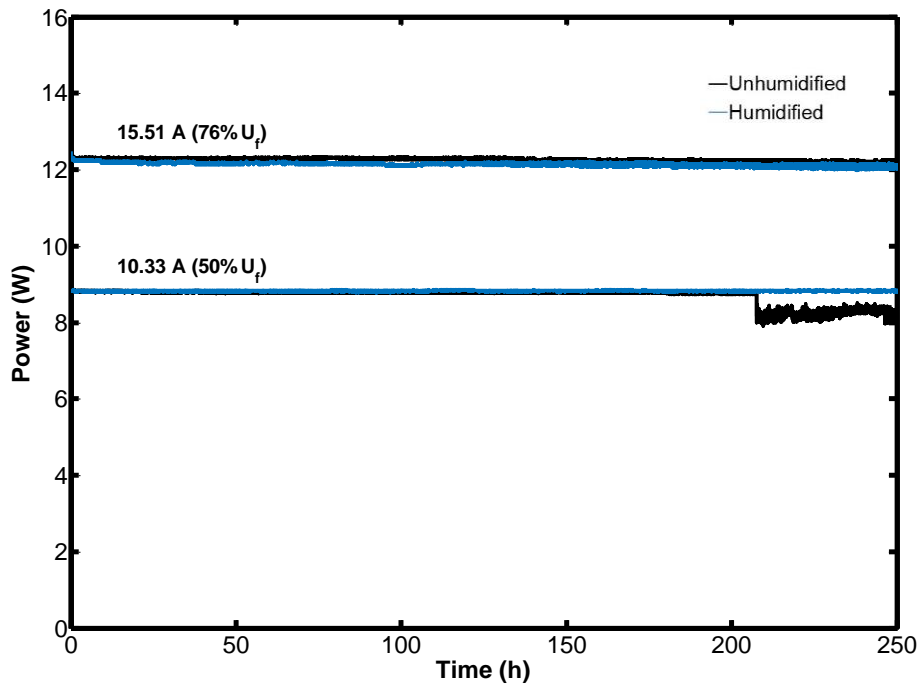


*Figure 34: Degradation rates for cells running with and without water at different utilizations.*

There is little difference between the humidified and unhumidified cells at the higher utilization and current density. This is likely due to the fact that at this higher utilization and current density there is less unconverted methane to form coke and there is more water produced via the oxidation of hydrogen than at the lower current density, so that adding more water to the stream does not significantly affect the performance of the cell. At the lower utilization and current density, however, the failure that occurred without water was likely due to coking caused by a

higher level of unconverted methane. The water addition obviously reduced coking and degradation, as suggested by the more stable operation. An increase in the amount of water in the cell appears to decrease the risk of cell failure due to carbon deposition. This is consistent with the notion that at lower fuel utilization when there is a higher coke formation rate (Figure 32), water has a beneficial effect on reduced coking via the cleansing reaction indicated in Eq. (35).

#### **4.4 Mass Spectrometry Analysis on the Outlet Gas of the Single-Cell SOFC**

The fourth objective was to analyze the outlet gas composition of a single-cell SOFC running on biogas under different operating conditions. This analysis was performed when the cell was running on 45:55 CH<sub>4</sub>:CO<sub>2</sub> at 900°C under both OCV and under a load. Figure 35 shows how the composition of each species changes as the load increases. The cell was held at each current value for five minutes to ensure steady-state. The changes in mole fraction of each of the species were expected except for that of methane. A potential reason for the mole fraction of methane increasing as the load increased is because the gas cooled slightly as it passed through the capillary tube into the mass spectrometer (the capillary was heated to 100°C). This may have caused the CO<sub>2</sub> and H<sub>2</sub> to reform CH<sub>4</sub> as the amount of CO<sub>2</sub> increased.

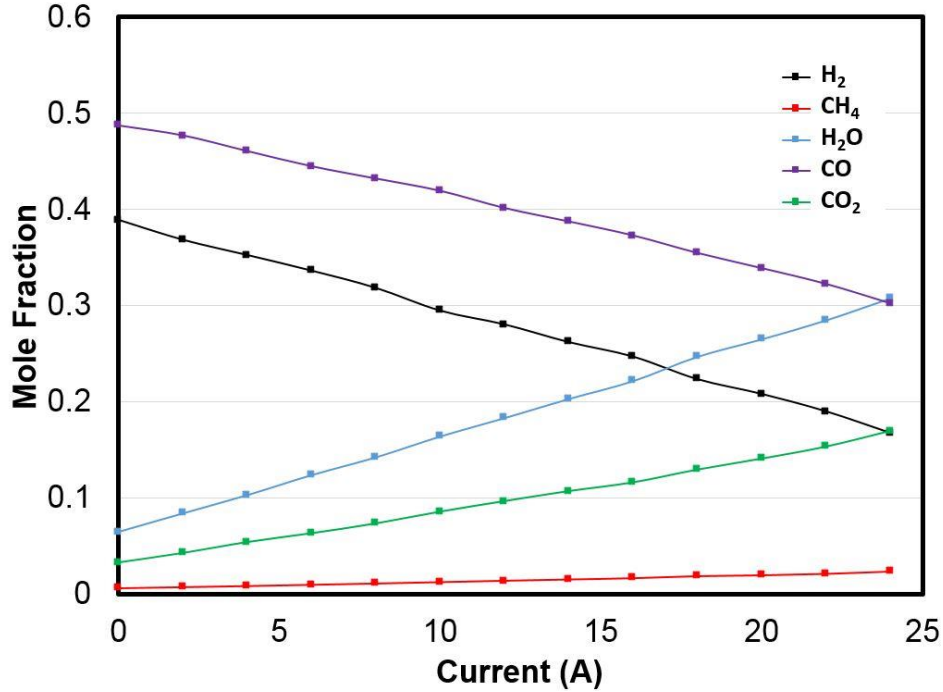


*Figure 35: Change in composition of species for incremental current values.*

When the current was 0, the cell was under OCV, and all reactions (dry reforming and reverse water gas shift) were presumably at DR and RWGS equilibrium. According to the thermodynamic analysis presented in section 3.2, the compositions of each species at OCV/equilibrium are as follows:

$$x_{\text{CH}_4,e} = 0.0086; x_{\text{CO}_2,e} = 0.0207; x_{\text{H}_2\text{O},e} = 0.0415; x_{\text{H}_2,e} = 0.4231; x_{\text{CO},e} = 0.5061.$$

These values are similar to the values shown in Figure 35 at OCV, but they are not identical. For example, the measured CO mole fraction is about 0.02 less than the theoretical, and the measured CO<sub>2</sub> and H<sub>2</sub>O mole fractions are about 0.03 more than the theoretical. For the theoretical analysis, the enthalpy of the reactions ( $\Delta H_{OR}^o$ ) was assumed to be constant with temperature, which could explain the difference between theoretical and measured OCV/equilibrium values because in reality, the enthalpy is a function of temperature.

$$\Delta H_T^0 = \Delta H_{298}^0 + \int_{T_{298}}^T \Delta C_p dT \quad (36)$$

The Gibbs free energy of the methane decomposition and the Boudouard reactions are provided as functions of temperature in equations 37 and 38 below, respectively (Ginsburg et al., 2005).

$$\Delta G^o = 58886.79 + 270.55T + 0.0311T^2 - (3.00 \times 10^{-6})T^3 + \frac{291405.7}{T} - 54.598T \ln(T) \quad (37)$$

$$\Delta G^o = -188030.19 + 402.82T + 0.00524T^2 + \frac{828509.9}{T} - 32.026T \ln(T) \quad (38)$$

As discussed in Chapter 2 and shown in Figure 36, the oxidation of both H<sub>2</sub> and CO generate power. Due to the slightly larger rate of oxidation of H<sub>2</sub> than CO, the total power generated comes slightly more from H<sub>2</sub> than CO.

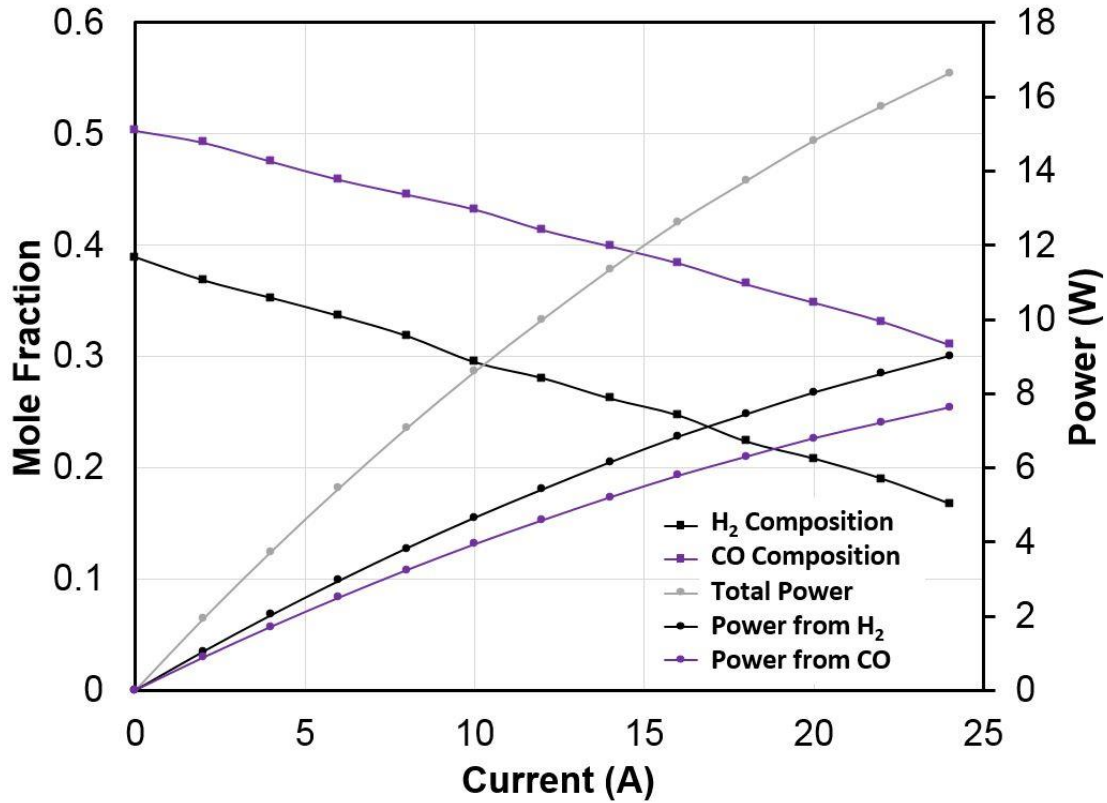


*Figure 36: H<sub>2</sub> and CO composition and respective and total power generation for incremental current values.*

The MS was calibrated before running the experiment, however, there are many factors in the testing apparatus that could cause errors. Due to this concern, all H<sub>2</sub> and CO mole fractions obtained in the MS analysis were fitted to the calibration curve shown in Figure 26.

#### 4.5 Effects of 45:55 CH<sub>4</sub>:CO<sub>2</sub> Fuel Through a 5-Cell SOFC Assembly

The fifth objective was to operate a 5-cell SOFC stack on the biogas conditions proven to be successful thus far. These conditions were 45:55 CH<sub>4</sub>:CO<sub>2</sub> and 76% fuel utilization at 900°C.

Figure 37 shows a polarization curve for the 5-cell stack running on these conditions.

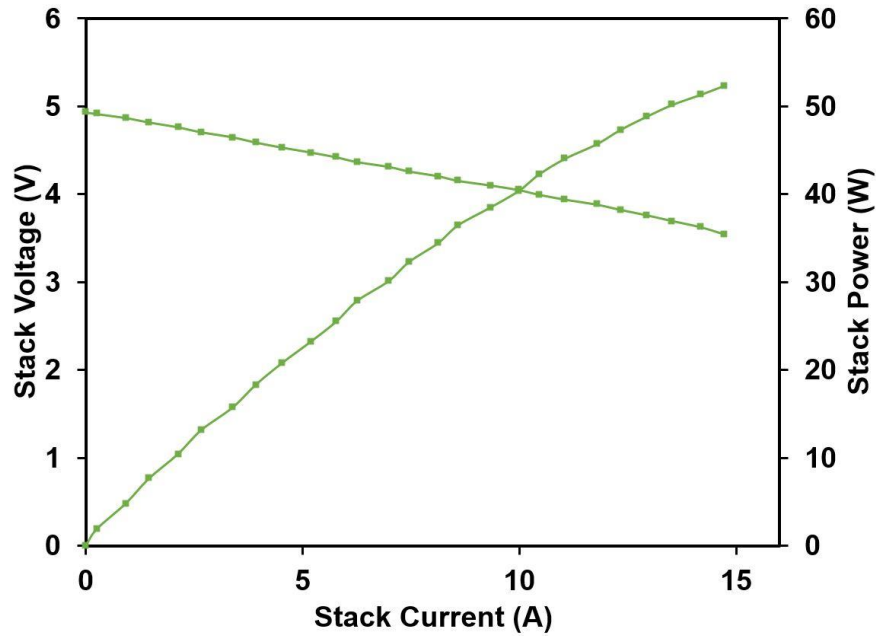


*Figure 37: Polarization curve for 5-cell stack on biogas.*

As shown in Figure 37, the 5-cell stack achieved a power of about 52 watts. If there were no losses throughout the stack, the power simply be the product of the number of cells and the power each cell produces. If, according to previous results (Figure 32), each cell is assumed to produce 12 watts, a 5-cell stack with no additional losses would produce a power of 60 watts. The slightly lower power produced in the stack is reasonable, and indicates that scaling up this SOFC system fed by biogas to eventually become a larger-scale, commercialized unit is entirely feasible.

## 5. Conclusions and Commercialization Potential

### 5.1 Conclusions

When looking at the results of the single-cell and 5-cell testing, it is clear that synthetic biogas can be fed through an SOFC to generate electricity. The most successful operating conditions were an operating temperature of 900°C, a biogas composition of 45:55 CH<sub>4</sub>:CO<sub>2</sub> and a high fuel utilization, at or above 76%. Under these conditions, the cell produced high power (12 watts per cell), and demonstrated long lifetime (estimated as about 7,000 hours before 10% degradation). It was also observed that adding water to the feed improved the lifetime of the SOFC operating at a low fuel utilization (50%). The mass spectrometer analysis confirmed the theoretical thermodynamic analysis due to the species' concentrations shown at OCV, and the relationship between the H<sub>2</sub> and CO concentrations and the current being drawn. The scaled-up 5-cell stack operating under 45:55 CH<sub>4</sub>:CO<sub>2</sub> and 900°C achieved a power of about 52 watts, suggesting that scaled-up units for practical applications have potential.

Based on the results obtained in this study, a 25-cell SOFC stack running on biogas under the conditions specified above has the potential to produce about 200 watts assuming the stack would experience about 30% losses. If the lifetime of the system was assumed to be about 10,000 hours, the energy rating for a 25-cell SOFC stack running on biogas would be 2,000 kWh.

### 5.2 Commercialization Potential

As discussed in Section 2.2, biogas infrastructure is readily available in many rural and developing countries around the world, and is currently used for cooking and heating. An SOFC would utilize the current infrastructure, but also introduce a clean and convenient way to

generate electricity. A small school in a village in Chhattisgarh, India uses about 465 kWh of electricity per year (Sen and Bhattacharyya, 2014). If the 2,000 kWh 25-cell biogas SOFC were to be utilized by the school, there are three implementation scenarios that have potential to be successful.

The first scenario would be to utilize solely the SOFC system. This would be the simplest model, as it capitalizes on the current infrastructure available, biogas. For this model, the SOFC would run constantly on about 7.5 m<sup>3</sup> of biogas per day until the point at which cell degradation causes poor SOFC performance. According to the results from this study, and assuming a maximum constant load of 54 watts for 10,000 hours, this would allow for a 14-18 month lifetime of the system. On average, this would generate a constant power supply to provide adequate electricity for the school's current needs for 14-18 months.

The second scenario would be to create an SOFC-battery hybrid system. Adding the battery to the system would allow for the energy produced in the SOFC to be stored in the battery for later use, allowing it to run under steady conditions despite varying demand during the day. Storing the energy could extend the lifetime of the SOFC to be longer than 14-18 months because it would be operating at a lower power density under stable conditions than under varying conditions throughout the day as the demand varies. If the school uses 465 kWh per year, the daily energy consumption is 1.6 kWh per day. The SOFC would thus only need to run for 6.5 hours each day to generate this much electricity. After the SOFC runs for 6.5 hours, it could be turned off until the battery needs recharging. This model could extend the lifetime of the SOFC to be about 4 years. However, in reality, there is a tradeoff between lifetime and cycling, which generally leads to faster degradation. With the SOFC being turned on and off every time the battery needs recharging, there is a great deal of mechanical stress on the cells and the system.

This would potentially require the SOFC to undergo cycling maintenance every 500 hours or so, but the overall lifetime of the SOFC in an SOFC-battery hybrid system could be greater than that of solely an SOFC system. On the other hand, an alternate way to extend the life is for the cell to operate steadily under a lower load, or alternately the cost of the unit could be decreased by utilizing a smaller unit.

The third scenario would be to implement a solar-SOFC-battery hybrid system. This system would first utilize a solar panel when the conditions are appropriate (i.e., sunlight), and then, when the conditions are not ideal for the solar panel, the system would tap into the energy stored in the battery from the SOFC. The SOFC-battery system would be similar to that explained above in that the SOFC would run for about 6.5 hours per day to charge the battery, but because the solar panel is also present and assumed to be utilizable 25% of the uptime of the school, the SOFC lifetime now extends to about 5 years. Alternately, again a smaller SOFC unit would suffice.

An economic analysis for each scenario would be needed to determine the most cost effective way to balance the lifetime and cycling maintenance of the SOFC with the capital, operational, and total costs. On the consumer end, if the system were to be large enough, a utility model where a community or non-governmental organization rents or purchases the system at a fixed cost would allow residents to pay a marginal amount for a clean form of electricity.

### **5.3 Recommendations for Future Work**

The next step in the work would be to obtain actual biogas samples from a local digester. These samples could be analyzed to determine their gas composition, and then fed through a sulfur filter to filter out the  $H_2S$  and any other impurities that could harm the SOFC. If the composition

of water in the sample is not significant, water could be added to the sample to improve the lifetime, as shown in Figure 34 above.

To potentially decrease the cost associated with a 25-cell stack system, the biogas could be heated to 900°C externally, allowing the SOFC itself to run on the H<sub>2</sub> and CO at 700°C instead of 900°C. This process could be designed and tested with single cells to determine its feasibility compared to operating the SOFC at 900°C.

More scale-up testing could be completed with synthetic biogas. Lifetime data could be obtained with the 5-cell stack, especially a fuel utilization and water addition versus lifetime matrix, similar to the single-cell tests explained in sections 4.2 and 4.3. Once operating conditions are optimized for synthetic biogas in the 5-cell stack, actual biogas samples could be tested in the 5-cell stack with the sulfur filter. A 25-cell stack could then be tested with both synthetic biogas and an actual biogas sample to provide data for a unit with potential for commercialization.

## References

- Anaerobic Digestion. Renewable Energy Concepts*. Retrieved 23 March 2016, from <http://www.renewable-energy-concepts.com/biomass-bioenergy/biogas-basics/anaerobic-digestion.html>
- Assabumrungrat, S., Laosiripojana, N., & Piroonlerkgul, P.(2006). Determination of the boundary of carbon formation for dry reforming of methane in a solid oxide fuel cell, *159*, 1274–1282. <http://doi.org/10.1016/j.jpowsour.2005.12.010>
- Baker, R., & Zhang, J.(2011). *Proton Exchange Membrane or Polymer Electrolyte Membrane (PEM) Fuel Cells. The Electrochemical Society*. Retrieved 23 March 2016, from <http://knowledge.electrochem.org/encycl/art-f04-fuel-cells-pem.htm>
- Biogas Composition. Renewable Energy Concepts*. Retrieved 23 March 2016, from <http://www.renewable-energy-concepts.com/biomass-bioenergy/biogas-basics/gas-composition.html>
- Bond, T., & Templeton, M. R.(2011). History and future of domestic biogas plants in the developing world. *Energy for Sustainable Development*, *15*(4), 347–354. <http://doi.org/10.1016/j.esd.2011.09.003>
- Carlowicz, M. *World of Change: Global Temperatures. NASA Earth Observatory*. Retrieved 22 May 2015, from <http://earthobservatory.nasa.gov/Features/WorldOfChange/decadaltemp.php>
- Cropgen,. *Renewable energy from crops and agrowastes*. Retrieved 1 June 2015, from <http://www.cropgen.soton.ac.uk/deliverables.htm>
- El-Mashad, H. M., & Zhang, R. (2010). Biogas production from co-digestion of dairy manure and food waste. *Bioresource Technology*, *101*(11), 4027. <http://doi.org/10.1016/j.biortech.2010.01.027>
- EPA,. *Methane Emissions*. Retrieved 25 May 2015, from <http://epa.gov/climatechange/ghgemissions/gases/ch4.html>
- FAO,. *Energy in the World Economy*. Retrieved 22 May 2015, from <http://www.fao.org/docrep/003/x8054e/x8054e04.htm>
- Fehrenbacher, K.(2013). *Apple now powering its cloud with solar panels, fuel cells (photos). Gigaom*. Retrieved 23 March 2016, from <https://gigaom.com/2013/03/21/apple-now-powering-its-cloud-with-solar-panels-fuel-cells-photos/>
- Fitzsimmons, A.(2013). *The Bloom is Off Bloom Energy. Institute for Energy Research*. Retrieved 23 March 2016, from <http://instituteforenergyresearch.org/analysis/the-bloom-is-off-bloom-energy/>

- Fogler, H., Aguilar Ortega, M., & Ramírez López, R. (2008). *Elementos de ingeniería de las reacciones químicas*. Naucalpan de Juárez, México.: Pearson Educación.
- Fuel Cell Energy,. *How do Fuel Cells Work?*. Retrieved 25 May 2015, from <http://www.fuelcellenergy.com/why-fuelcell-energy/how-do-fuel-cells-work/>
- Fuel Cell Technology Market by Types*(2014). *Markets and Markets*. Retrieved 24 March 2016, from <http://www.marketsandmarkets.com/Market-Reports/fuel-cell-market-348.html>
- Garrison, E. *Solid Oxide Fuel Cells. IIT*. Retrieved 25 May 2015, from <http://mypages.iit.edu/~smart/garrear/fuelcells.htm>
- Ginsburg, J. M., Piña, J., El Solh, T., & De Lasa, H. I. (2005). Coke formation over a nickel catalyst under methane dry reforming conditions: Thermodynamic and kinetic models. *Industrial & engineering chemistry research*, 44(14), 4846-4854
- Goodwin, D. G., Zhu, H., Colclasure, A. M., and Kee, R. J. “Modeling Electrochemical Oxidation of Hydrogen on Ni-YSZ Pattern Anodes,” *J. Electrochem. Soc.*, 156, B1004-B1021 (2009).
- Hecht, E. S., Gupta, G. K., Zhu, H., Dean, A. M., Kee, R. J., Maier, L., & Deutschmann, O.(2005). Methane reforming kinetics within a Ni-YSZ SOFC anode support. *Applied Catalysis A: General*, 295(1), 40–41. <http://doi.org/10.1016/j.apcata.2005.08.003>
- Homel, M., Gür, T. M., Koh, J. H., & Virkar, A. V. (2010). Carbon monoxide-fueled solid oxide fuel cell. *Journal of Power Sources*, 195(19), 6367-6372.
- Introduction to Fuel Cell Technology - Overview*(2012). *NPTEL*. Retrieved 23 March 2016, from <http://www.nptel.ac.in/courses/103102015/2>
- Janardhanan, V. & Deutschmann, O. (2007). Modeling of Solid-Oxide Fuel Cells. *Zeitschrift Für Physikalische Chemie*, 221(4), 443-478. <http://dx.doi.org/10.1524/zpch.2007.221.4.443>
- Lanzini, A., Leone, P., Guerra, C., Smeacetto, F., Brandon, N. P., & Santarelli, M(2013). Durability of anode supported Solid Oxides Fuel Cells (SOFC) under direct dry-reforming of methane. *Chemical Engineering Journal*, 220, 254–263. <http://doi.org/10.1016/j.cej.2013.01.003>
- Laosiripojana, N., & Assabumrungrat, S(2007). Catalytic steam reforming of methane, methanol, and ethanol over Ni/YSZ: The possible use of these fuels in internal reforming SOFC. *Journal of Power Sources*, 163(2), 943–951. <http://doi.org/10.1016/j.jpowsour.2006.10.006>
- Mebarki, B., Adouane, B., Khaldi, F., Dehimi, S., & Haddad, D(2015). ScienceDirect Theoretical estimation of the production of biogas from the landfill of Batna city and its electrical conversion by a SOFC. *International Journal of Hydrogen Energy*, 40(39), 13799–13805. <http://doi.org/10.1016/j.ijhydene.2015.03.062>

- Mermelstein, J., Millan, M., & Brandon, N. P.(2011). The interaction of biomass gasification syngas components with tar in a solid oxide fuel cell and operational conditions to mitigate carbon deposition on nickel-gadolinium doped ceria anodes. *Journal of Power Sources*, 196(11), 5027–5034. <http://doi.org/10.1016/j.jpowsour.2011.02.011>
- Muzenda, E(2014). Bio-methane Generation from Organic Waste : A Review, *II*, 4.
- Olivier, M(2008). *Fuel Cell Characterization*. Presentation, Academie Universitaire Wallonie-Bruxelles.
- Papadam, T., Goula, G., & Yentekakis, I. V(2012). Long-term operation stability tests of intermediate and high temperature Ni-based anodes' SOFCs directly fueled with simulated biogas mixtures. *International Journal of Hydrogen Energy*, 37(21), 16680–16685. <http://doi.org/10.1016/j.ijhydene.2012.02.147>
- Population Reference Bureau,. *Human Population: Population Growth*. Retrieved 3 June 2015, from <http://www.prb.org/Publications/Lesson-Plans/HumanPopulation/PopulationGrowth.aspx>
- Protonex,. *Solid Oxide Fuel Cell Technology*. Retrieved 25 May 2015, from <http://www.protonex.com/technology/solid-oxide-fuel-cell/>
- Rayment, C(2003). Introduction to Fuel Cell Technology, 19–38. <http://doi.org/10.1.1.129.3231>
- SAE International., (2015). *Fuel Cell Technology Showcase - History of Fuel Cells*. Retrieved 10 June 2015, from <http://www.sae.org/fuelcells/fuelcells-history.htm>
- Sen, R. & Bhattacharyya, S. (2014). Off-grid electricity generation with renewable energy technologies in India: An application of HOMER. *Renewable Energy*, 62, 388-398. <http://dx.doi.org/10.1016/j.renene.2013.07.028>
- Services of SRC's Wastewater Treatment Unit*(2012). *Scientific Research Council*. Retrieved 22 March 2016, from <http://www.src.gov.jm/services-wastewater-treatment-unit/>
- Shiratori, Y., Ijichi, T., Oshima, T., & Sasaki, K(2010). Internal reforming SOFC running on biogas. *International Journal of Hydrogen Energy*, 35(15), 7905–7912. <http://doi.org/10.1016/j.ijhydene.2010.05.064>
- Standardization in SOFC Testing. Fuel Cell Markets*. Retrieved 23 March 2016, from <http://www.fuelcellmarkets.com/content/images/articles/WP1.pdf>
- Taherzadeh, Mohammad. "Waste Biorefinery: Biogas In Vietnam". *University of Boras*. N.p., 2012. Web. 23 Mar. 2016.
- Technologies*(2016). *Fuel Cell Today*. Retrieved 23 March 2016, from <http://www.fuelcelltoday.com/technologies>

- The Biodigester and its Benefits*(2014). *TransformAsia*. Retrieved 22 March 2016, from <http://www.transformasia.us/biodigester-and-it-benefits/>
- Tubular SOFC, Solid Oxide Fuel Cell Technology*. *Acumentrics*. Retrieved 23 March 2016, from <http://www.acumentrics.com/sofc-products-fuel-cell-technology.htm>
- U.S. Department of Energy, Office of Fossil Energy, (2004). *Fuel Cell Handbook* (pp. 2-12). Morgantown, West Virginia.
- Vindis, P., & Mursec, B(2009). The impact of mesophilic and thermophilic anaerobic digestion on biogas production. *Journal of Achievements ...*, 36(2), 197. Retrieved from [http://www.journalamme.org/papers\\_vol36\\_2/36210.pdf](http://www.journalamme.org/papers_vol36_2/36210.pdf)
- Waldemar Bujalski, Chinnan M. Dikwal, Kevin Kendall, “Cycling of three solid oxide fuel cell types,” *Journal of Power Sources*, Volume 171, Issue 1, 19 September 2007, Pages 96-100.
- Wang, Y., Chen, K. S., Mishler, J., Cho, S. C., & Adroher, X. C(2011). A review of polymer electrolyte membrane fuel cells: Technology, applications, and needs on fundamental research. *Applied Energy*, 88(4), 981–1007. <http://doi.org/10.1016/j.apenergy.2010.09.030>
- Yi, Y., Rao, A. D., Brouwer, J., & Samuelsen, G. S(2005). Fuel flexibility study of an integrated 25 kW SOFC reformer system. *Journal of Power Sources*, 144(1), 1. <http://doi.org/10.1016/j.jpowsour.2004.11.068>

## Appendices

### Appendix A

The ionization probability was used in conjunction with the mass spectrometer to calculate the partial pressures of each gas species exiting the cell.

Page 2

## Application Note

### IONIZATION PROBABILITY

| SUBSTANCE             | FORMULA   | RELATIVE IONIZATION GAUGE SENSITIVITY Signal/Signal Nitrogen |
|-----------------------|---|--|
| Acetone               | (CH <sub>3</sub> ) <sub>2</sub> CO                            | 3.6  |
| Air                   |   | 1.0  |
| Ammonia               | NH <sub>3</sub>   | 1.3  |
| Argon                 | Ar  | 1.2  |
| Benzene               | C <sub>6</sub> H <sub>6</sub>                                 | 5.9  |
| Benzoic acid          | C <sub>6</sub> H <sub>5</sub> COOH                            | 5.5  |
| Bromine               | Br  | 3.8  |
| Butane                | C <sub>4</sub> H <sub>10</sub>                                | 4.9  |
| Carbon dioxide        | CO <sub>2</sub>   | 1.4  |
| Carbon disulfide      | CS <sub>2</sub>   | 4.8  |
| Carbon monoxide       | CO  | 1.05   |
| Chlorobenzene         | C <sub>6</sub> H <sub>5</sub> Cl                              | 7.0  |
| Chloroethane          | C <sub>2</sub> H <sub>5</sub> Cl                              | 4.0  |
| Chloromethane         | CH <sub>3</sub> Cl  | 3.1  |
| Cyclohexylene         | C <sub>6</sub> H <sub>12</sub>                                | 6.4  |
| Deuterium             | D <sub>2</sub>  | 0.35   |
| Dichlorofluoromethane | CCl <sub>2</sub> F <sub>2</sub>                               | 2.7  |
| Dichloromethane       | CH <sub>2</sub> Cl <sub>2</sub>                               | 3.7  |
| Dinitrobenzene        | C <sub>6</sub> H <sub>4</sub> (NO <sub>2</sub> ) <sub>2</sub> | 7.8  |
| Ethane                | C <sub>2</sub> H <sub>6</sub>                                 | 2.6  |
| Ethanol               | C <sub>2</sub> H <sub>5</sub> OH                              | 3.8  |
| Ethylene Oxide        | (CH <sub>2</sub> ) <sub>2</sub> O                             | 2.5  |
| Helium                | He  | 0.14   |
| Hexane                | C <sub>6</sub> H <sub>14</sub>                                | 6.6  |
| Hydrogen              | H <sub>2</sub>  | 0.44   |
| Hydrogen chloride     | HCl   | 1.6  |
| Hydrogen fluoride     | HF  | 1.4  |
| Hydrogen iodide       | HI  | 3.1  |
| Hydrogen sulfide      | H <sub>2</sub> S  | 2.2  |
| Krypton               | Kr  | 1.7  |
| Lithium               | Li  | 1.9  |
| Methane               | CH <sub>4</sub>   | 1.6  |
| Methanol              | CH <sub>3</sub> OH  | 1.8  |
| Neon                  | Ne  | 0.23   |
| Nitrogen              | N <sub>2</sub>  | 1.0  |
| Nitric oxide          | NO  | 1.2  |
| Nitrous oxide         | N <sub>2</sub> O  | 1.7  |

| SUBSTANCE           | FORMULA   | RELATIVE IONIZATION GAUGE SENSITIVITY Signal/Signal Nitrogen |
|---------------------|---|--|
| Oxygen              | O <sub>2</sub>  | 1  |
| n-Pentane           | C <sub>5</sub> H <sub>12</sub>                                | 6  |
| Phenol              | C <sub>6</sub> H <sub>5</sub> OH                              | 6.2  |
| Phosphine           | PH <sub>3</sub>   | 2.6  |
| Propane             | C <sub>3</sub> H <sub>8</sub>                                 | 3.7  |
| Silver perchlorate  | AgClO <sub>4</sub>  | 3.6  |
| Stannic iodide      | SnI <sub>4</sub>  | 6.7  |
| Sulfur dioxide      | SO <sub>2</sub>   | 2.1  |
| Sulfur hexafluoride | SF <sub>6</sub>   | 2.3  |
| Tetrachloromethane  | CCl <sub>4</sub>  | 6  |
| Toluene             | C <sub>6</sub> H <sub>5</sub> CH <sub>3</sub>                 | 6.8  |
| Trichloromethane    | CHCl <sub>3</sub>   | 4.8  |
| Trinitrobenzene     | C <sub>6</sub> H <sub>3</sub> (NO <sub>2</sub> ) <sub>3</sub> | 9  |
| Water               | H <sub>2</sub> O  | 1  |
| Xenon               | Xe  | 3  |
| Xylene              | C <sub>6</sub> H <sub>4</sub> (CH <sub>3</sub> ) <sub>2</sub> | 7.8  |

For further information, call your local MKS Sales Engineer or contact the MKS Applications Engineering Group at 800.227.8766.



App. Note #03/02 - 2/11  
© 2005 MKS Instruments, Inc.  
All rights reserved.

MKS Gas Analyzers  
Spectra Products, USA  
134 W. Rio Robles Drive  
San Jose, CA 95134  
408.750.0300

Spectra Products, UK  
Cowley Way  
Crews, Cheshire CW1 6AG  
+44.1270.250150

MKS Global Headquarters  
2 Tech Drive, Suite 201  
Andover, MA 01810  
978.545.5500  
800.227.8766 (in U.S.A.)  
www.mksinst.com

## Appendix B

A procedure was written into the Universal Data Acquisition (UDA) Software as shown below.

**Running - C:\UDA Data\TS 044 Bay 4\Courtney\Config Files\WQP\CO IV 900.dat**

File Action Schedule Help

| [on] Variable   | Value         | Graph  | Logging |
|---|---------------|--------|---------|
| <input checked="" type="checkbox"/> Cell Temp ai4 (control) | 22.1179107... | ACTIVE | on      |
| <input checked="" type="checkbox"/> Inlet Temp ai3          | 22.4058692... | ACTIVE | on      |
| <input checked="" type="checkbox"/> Outlet temp ai2         | 23.9028131... | ACTIVE | on      |
| <input type="checkbox"/> Out V Sense                        | 1.75680927... |        | on      |
| <input type="checkbox"/> In V Sense                         | 1.57166828... |        | on      |
| <input checked="" type="checkbox"/> Load Voltage Sense      | 0             | ACTIVE | on      |
| <input checked="" type="checkbox"/> Load Current            | 0             | ACTIVE | on      |
| <input type="checkbox"/> Duty Cycle                         | 0             |        | on      |
| <input type="checkbox"/> Anode N2 Flow                      | 0             |        | on      |
| <input type="checkbox"/> Anode H2 Flow                      | 0             |        | on      |
| <input type="checkbox"/> Cathode Flow                       | 0             |        | on      |
| <input checked="" type="checkbox"/> Cell Power              | 0             | ACTIVE | on      |
| <input type="checkbox"/> Anode CO2 Flow                     | 0             |        | on      |
| <input type="checkbox"/> Anode CH4 Flow                     | 0             |        | on      |

| Register | Value |
|----------|-------|
| REG0     | 0     |
| REG1     | 0     |
| REG2     | 0     |
| REG3     | 0     |
| REG4     | 0     |
| REG5     | 0     |
| REG6     | 0     |
| REG7     | 0     |
| REG8     | 0     |
| REG9     | 0     |
| REG10    | 0     |
| REG11    | 0     |
| REG12    | 0     |
| REG13    | 0     |
| REG14    | 0     |
| REG15    | 0     |

| Name             | Tag  | Details           |
|------------------|------|-------------------|
| NiDAQDevice0     | Dev3 | Ok                |
| AlicatFlowGroup1 | CDM1 | Ok                |
| AmrelLoad2       | CDM3 | Ok                |
| BasicPIDLoop3    | ---  | Out: 0%, Scaled:0 |
| Timer4           | ---  | 0 [0]             |

| Id | Device           | Operation                         | Time (...) | Schedule Tag / Co |
|----|------------------|-----------------------------------|------------|-------------------|
| 1  | AlicatFlowGroup1 | Set Fixed Flow(Nitrogen (A), 0.1) | 0          |                   |
| 2  | ----             | Delay                             | 1          |                   |
| 3  | AlicatFlowGroup1 | Set Fixed Flow(Hydrogen (B), 0.1) | 0          |                   |
| 4  | AlicatFlowGroup1 | Set Fixed Flow(Cathode (C), 2)    | 0          |                   |
| 5  | ----             | Delay                             | 15         | 1                 |
| 6  | BasicPIDLoop3    | Start()                           | 0          |                   |
| 7  | BasicPIDLoop3    | Update Set Point(900)             | 0          |                   |
| 8  | NiDAQDevice0     | Wait (Temp 4 (ai4)) > 897         | 0          |                   |
| 9  | ----             | Delay                             | 180        |                   |
| 10 | AmrelLoad2       | Send String Command(util:range 1) | 0          | 2                 |
| 11 | AmrelLoad2       | Run VI Curve(0.65, 25, 0.2, 0)    | 0          | 2                 |
| 12 | AmrelLoad2       | Turn Load OFF()                   | 0          |                   |
| 13 | AmrelLoad2       | Turn ON CC Load(18.09)            | 0          | 3                 |
| 14 | ----             | Delay                             | 60         | 3                 |
| 15 | AmrelLoad2       | Turn Load OFF()                   | 0          |                   |
| 16 | AmrelLoad2       | Run VI Curve(0.65, 25, 0.2, 0)    | 0          | 4                 |

Start Stop Start At Time left in step (min):

C:\Program Files\Protonex\Universal Data Acquire

Running - C:\UDA Data\TS 044 Bay 4\Courtney\Config Files\MQP\CO IV 900.dat

File Action Schedule Help

| [on] Variable   | Value         | Graph  | Logging | Register | Value |
|---|---------------|--------|---------|----------|-------|
| <input checked="" type="checkbox"/> Cell Temp ai4 (control) | 22.3823664... | ACTIVE | on      | REG0     | 0     |
| <input checked="" type="checkbox"/> Inlet Temp ai3          | 21.9889736... | ACTIVE | on      | REG1     | 0     |
| <input checked="" type="checkbox"/> Outlet temp ai2         | 23.4145165... | ACTIVE | on      | REG2     | 0     |
| <input type="checkbox"/> Out V Sense                        | 1.75230326... |        | on      | REG3     | 0     |
| <input type="checkbox"/> In V Sense                         | 1.57262211... |        | on      | REG4     | 0     |
| <input checked="" type="checkbox"/> Load Voltage Sense      | 0             | ACTIVE | on      | REG5     | 0     |
| <input checked="" type="checkbox"/> Load Current            | 0             | ACTIVE | on      | REG6     | 0     |
| <input type="checkbox"/> Duty Cycle                         | 0             |        | on      | REG7     | 0     |
| <input type="checkbox"/> Anode N2 Flow                      | 0             |        | on      | REG8     | 0     |
| <input type="checkbox"/> Anode H2 Flow                      | 0             |        | on      | REG9     | 0     |
| <input type="checkbox"/> Cathode Flow                       | 0             |        | on      | REG10    | 0     |
| <input checked="" type="checkbox"/> Cell Power              | 0             | ACTIVE | on      | REG11    | 0     |
| <input type="checkbox"/> Anode CO2 Flow                     | 0             |        | on      | REG12    | 0     |
| <input type="checkbox"/> Anode CH4 Flow                     | 0             |        | on      | REG13    | 0     |
|   |               |        |         | REG14    | 0     |
|   |               |        |         | REG15    | 0     |

| Name             | Tag  | Details           |
|------------------|------|-------------------|
| NiDAQDevice0     | Dev3 | OK                |
| AlicatFlowGroup1 | COM1 | OK                |
| AmrelLoad2       | COM3 | OK                |
| BasicPIDLoop3    | ---  | Out: 0%, Scaled:0 |
| Timer4           | ---  | 0 [0]             |

| Id | Device           | Operation                                | Time (...) | Schedule Tag / Co |
|----|------------------|--|------------|-------------------|
| 11 | AmrelLoad2       | Run VI Curve(0.65, 25, 0.2, 0)           | 0          | 2                 |
| 12 | AmrelLoad2       | Turn Load OFF()                          | 0          |                   |
| 13 | AmrelLoad2       | Turn ON CC Load(18.09)                   | 0          | 3                 |
| 14 | ---              | Delay                                    | 60         | 3                 |
| 15 | AmrelLoad2       | Turn Load OFF()                          | 0          |                   |
| 16 | AmrelLoad2       | Run VI Curve(0.65, 25, 0.2, 0)           | 0          | 4                 |
| 17 | AmrelLoad2       | Turn Load OFF()                          | 0          |                   |
| 18 | ---              | Delay                                    | 30         |                   |
| 19 | AlicatFlowGroup1 | Set Fixed Flow(Methane (E), 0.09)        | 0          |                   |
| 20 | AlicatFlowGroup1 | Set Fixed Flow(Carbon Dioxide (D), 0.11) | 0          |                   |
| 21 | AlicatFlowGroup1 | Set Fixed Flow(Hydrogen (B), 0)          | 0          |                   |
| 22 | AlicatFlowGroup1 | Set Fixed Flow(Nitrogen (A), 0)          | 0          |                   |
| 23 | AlicatFlowGroup1 | Set Fixed Flow(Cathode (C), 2)           | 0          |                   |
| 24 | ---              | Delay                                    | 15         |                   |
| 25 | AmrelLoad2       | Run VI Curve(0.7, 25, 0.2, 0)            | 0          | 5                 |
| 26 | AmrelLoad2       | Turn Load OFF()                          | 0          |                   |

Start Stop Start At Time left in  Running - C:\UDA Data\TS 044 Bay 4\Courtney\Config Files\MQP\CC

Running - C:\UDA Data\TS 044 Bay 4\Courtney\Config Files\WQP\CO IV 900.dat

File Action Schedule Help

| [on] Variable   | Value         | Graph  | Logging | Register | Value |
|---|---------------|--------|---------|----------|-------|
| <input checked="" type="checkbox"/> Cell Temp ai4 (control) | 22.4815373... | ACTIVE | on      | REG0     | 0     |
| <input checked="" type="checkbox"/> Inlet Temp ai3          | 22.0219950... | ACTIVE | on      | REG1     | 0     |
| <input checked="" type="checkbox"/> Outlet temp ai2         | 23.4972786... | ACTIVE | on      | REG2     | 0     |
| <input type="checkbox"/> Out V Sense                        | 1.75138232... |        | on      | REG3     | 0     |
| <input type="checkbox"/> In V Sense                         | 1.57249055... |        | on      | REG4     | 0     |
| <input checked="" type="checkbox"/> Load Voltage Sense      | 0             | ACTIVE | on      | REG5     | 0     |
| <input checked="" type="checkbox"/> Load Current            | 0             | ACTIVE | on      | REG6     | 0     |
| <input type="checkbox"/> Duty Cycle                         | 0             |        | on      | REG7     | 0     |
| <input type="checkbox"/> Anode N2 Flow                      | 0             |        | on      | REG8     | 0     |
| <input type="checkbox"/> Anode H2 Flow                      | 0             |        | on      | REG9     | 0     |
| <input type="checkbox"/> Cathode Flow                       | 0             |        | on      | REG10    | 0     |
| <input checked="" type="checkbox"/> Cell Power              | 0             | ACTIVE | on      | REG11    | 0     |
| <input type="checkbox"/> Anode CO2 Flow                     | 0             |        | on      | REG12    | 0     |
| <input type="checkbox"/> Anode CH4 Flow                     | 0             |        | on      | REG13    | 0     |
|   |               |        |         | REG14    | 0     |
|   |               |        |         | REG15    | 0     |

| Name             | Tag  | Details           |
|------------------|------|-------------------|
| NiDaqDevice0     | Dev3 | Ok                |
| AlicatFlowGroup1 | COM1 | Ok                |
| AmrelLoad2       | COM3 | Ok                |
| BasicPIDLoop3    | ---  | Out: 0%, Scaled:0 |
| Timer4           | ---  | 0 [0]             |

| Id | Device           | Operation                         | Time (...) | Schedule Tag / Co |
|----|------------------|-----------------------------------|------------|-------------------|
| 26 | AmrelLoad2       | Turn Load OFF()                   | 0          |                   |
| 27 | AmrelLoad2       | Turn ON CC Load(18.09)            | 0          | 6                 |
| 28 | ----             | Loop (forever)                    | ----       | 6                 |
| 29 | Timer4           | If (Value) > 300572               | 0          | 6                 |
| 30 | ----             | Break Out                         | ----       | 6                 |
| 31 | ----             | End If                            | ----       | 6                 |
| 32 | AmrelLoad2       | If (Power) < 1.65                 | 0          | 6                 |
| 33 | ----             | Goto Tag: 5                       | ----       | 6                 |
| 34 | ----             | End If                            | ----       | 6                 |
| 35 | ----             | End Loop                          | ----       | 6                 |
| 36 | AmrelLoad2       | Turn Load OFF()                   | 0          |                   |
| 37 | AmrelLoad2       | Run VI Curve(0.7, 25, 0.2, 0)     | 0          | 7                 |
| 38 | AmrelLoad2       | Turn Load OFF()                   | 0          |                   |
| 39 | ----             | Delay                             | 30         |                   |
| 40 | AlicatFlowGroup1 | Set Fixed Flow(Nitrogen (A), 0.1) | 0          |                   |
| 41 | ----             | Delay                             | 1          |                   |

Start  Stop At Time left in step (min):

Running - C:\UDA Data\TS 044 Bay 4\Courtney\Config Files\MQP\CO IV 900.dat

File Action Schedule Help

| [on] Variable  | Value         | Graph  | Logging | Register | Value |
|--|---------------|--------|---------|----------|-------|
| <input checked="" type="checkbox"/> CellTemp ai4 (control) | 22.0972501... | ACTIVE | on      | REG0     | 0     |
| <input checked="" type="checkbox"/> Inlet Temp ai3         | 22.2696558... | ACTIVE | on      | REG1     | 0     |
| <input checked="" type="checkbox"/> Outlet temp ai2        | 23.6007313... | ACTIVE | on      | REG2     | 0     |
| <input type="checkbox"/> Out V Sense                       | 1.75243482... |        | on      | REG3     | 0     |
| <input type="checkbox"/> In V Sense                        | 1.57203008... |        | on      | REG4     | 0     |
| <input checked="" type="checkbox"/> Load Voltage Sense     | 0             | ACTIVE | on      | REG5     | 0     |
| <input checked="" type="checkbox"/> Load Current           | 0             | ACTIVE | on      | REG6     | 0     |
| <input type="checkbox"/> Duty Cycle                        | 0             |        | on      | REG7     | 0     |
| <input type="checkbox"/> Anode N2 Flow                     | 0             |        | on      | REG8     | 0     |
| <input type="checkbox"/> Anode H2 Flow                     | 0             |        | on      | REG9     | 0     |
| <input type="checkbox"/> Cathode Flow                      | 0             |        | on      | REG10    | 0     |
| <input checked="" type="checkbox"/> Cell Power             | 0             | ACTIVE | on      | REG11    | 0     |
| <input type="checkbox"/> Anode CO2 Flow                    | 0             |        | on      | REG12    | 0     |
| <input type="checkbox"/> Anode CH4 Flow                    | 0             |        | on      | REG13    | 0     |
|  |               |        |         | REG14    | 0     |
|  |               |        |         | REG15    | 0     |

| Name             | Tag  | Details           |
|------------------|------|-------------------|
| NiDaqDevice0     | Dev3 | Ok                |
| AlicatFlowGroup1 | COM1 | Ok                |
| AmrelLoad2       | COM3 | Ok                |
| BasicPIDLoop3    | ---  | Out: 0%, Scaled:0 |
| Timer4           | ---  | 0 [0]             |

| Id | Device           | Operation                             | Time (...) | Schedule Tag / Coi |
|----|------------------|---------------------------------------|------------|--------------------|
| 41 | ---              | Delay                                 | 1          |                    |
| 42 | AlicatFlowGroup1 | Set Fixed Flow(Hydrogen (B), 0.1)     | 0          |                    |
| 43 | AlicatFlowGroup1 | Set Fixed Flow(Methane (E), 0)        | 0          |                    |
| 44 | AlicatFlowGroup1 | Set Fixed Flow(Carbon Dioxide (D), 0) | 0          |                    |
| 45 | AlicatFlowGroup1 | Set Fixed Flow(Cathode (C), 2)        | 0          |                    |
| 46 | ---              | Delay                                 | 15         |                    |
| 47 | AmrelLoad2       | Run VI Curve(0.65, 25, 0.2, 0)        | 0          | 8                  |
| 48 | AmrelLoad2       | Turn Load OFF()                       | 0          |                    |
| 49 | AmrelLoad2       | Turn ON CC Load(18.09)                | 0          | 9                  |
| 50 | ---              | Delay                                 | 60         | 9                  |
| 51 | AmrelLoad2       | Turn Load OFF()                       | 0          |                    |
| 52 | AmrelLoad2       | Run VI Curve(0.65, 25, 0.2, 0)        | 0          | 10                 |
| 53 | ---              | Tag: 5                                | ---        |                    |
| 54 | AmrelLoad2       | Turn Load OFF()                       | 0          |                    |
| 55 | ---              | Delay                                 | 30         |                    |
| 56 | BasicPIDLoop3    | Stop()                                | 0          | 11                 |

Start Stop Start At Time left in step (min):

✓ ↑

Running - C:\UDA Data\TS 044 Bay 4\Courtney\Config Files\WQP\CO IV 900.dat

File Action Schedule Help

| [on] Variable   | Value         | Graph  | Logging | Register | Value |
|---|---------------|--------|---------|----------|-------|
| <input checked="" type="checkbox"/> Cell Temp ai4 (control) | 22.0889858... | ACTIVE | on      | REG0     | 0     |
| <input checked="" type="checkbox"/> Inlet Temp ai3          | 22.3563371... | ACTIVE | on      | REG1     | 0     |
| <input checked="" type="checkbox"/> Outlet temp ai2         | 23.7455650... | ACTIVE | on      | REG2     | 0     |
| <input type="checkbox"/> Out V Sense                        | 1.75296107... |        | on      | REG3     | 0     |
| <input type="checkbox"/> In V Sense                         | 1.57124071... |        | on      | REG4     | 0     |
| <input checked="" type="checkbox"/> Load Voltage Sense      | 0             | ACTIVE | on      | REG5     | 0     |
| <input checked="" type="checkbox"/> Load Current            | 0             | ACTIVE | on      | REG6     | 0     |
| <input type="checkbox"/> Duty Cycle                         | 0             |        | on      | REG7     | 0     |
| <input type="checkbox"/> Anode N2 Flow                      | 0             |        | on      | REG8     | 0     |
| <input type="checkbox"/> Anode H2 Flow                      | 0             |        | on      | REG9     | 0     |
| <input type="checkbox"/> Cathode Flow                       | 0             |        | on      | REG10    | 0     |
| <input checked="" type="checkbox"/> Cell Power              | 0             | ACTIVE | on      | REG11    | 0     |
| <input type="checkbox"/> Anode CO2 Flow                     | 0             |        | on      | REG12    | 0     |
| <input type="checkbox"/> Anode CH4 Flow                     | 0             |        | on      | REG13    | 0     |
|   |               |        |         | REG14    | 0     |
|   |               |        |         | REG15    | 0     |

| Name             | Tag  | Details           |
|------------------|------|-------------------|
| NiDAQDevice0     | Dev3 | Ok                |
| AlicatFlowGroup1 | COM1 | Ok                |
| AmrelLoad2       | COM3 | Ok                |
| BasicPIDLoop3    | ---  | Out: 0%, Scaled:0 |
| Timer4           | ---  | 0 [0]             |

| Id | Device           | Operation                             | Time (...) | Schedule Tag / Co |
|----|------------------|---------------------------------------|------------|-------------------|
| 49 | AmrelLoad2       | Turn ON CC Load(18.09)                | 0          | 9                 |
| 50 | ----             | Delay                                 | 60         | 9                 |
| 51 | AmrelLoad2       | Turn Load OFF()                       | 0          |                   |
| 52 | AmrelLoad2       | Run VI Curve(0.65, 25, 0.2, 0)        | 0          | 10                |
| 53 | ----             | Tag: 5                                | ----       |                   |
| 54 | AmrelLoad2       | Turn Load OFF()                       | 0          |                   |
| 55 | ----             | Delay                                 | 30         |                   |
| 56 | BasicPIDLoop3    | Stop()                                | 0          | 11                |
| 57 | NiDAQDevice0     | Wait (Temp 4 (ai4)) < 100             | 0          | 11                |
| 58 | AlicatFlowGroup1 | Set Fixed Flow(Methane (E), 0)        | 0          |                   |
| 59 | AlicatFlowGroup1 | Set Fixed Flow(Carbon Dioxide (D), 0) | 0          |                   |
| 60 | AlicatFlowGroup1 | Set Fixed Flow(Nitrogen (A), 0)       | 0          |                   |
| 61 | AlicatFlowGroup1 | Set Fixed Flow(Hydrogen (B), 0)       | 0          |                   |
| 62 | NiDAQDevice0     | Set Output(Safety (port1/line0), 0)   | 0          | 12                |
| 63 | ----             | Stop Polling and Script               | ----       | 12                |

Start Stop Start At Time left in step (min): [✓] [↑]

## Appendix C

The standard enthalpy and entropy values for each of the species analyzed in this work were gathered from the table below.

Standard Enthalpies of Formation & Standard Entropies of Common Compounds

| <i>Substance</i>                  | <i>State</i> | $\Delta H_f^\circ$<br>( $\frac{\text{kJ}}{\text{mol}}$ ) | $S^\circ$<br>( $\frac{\text{J}}{\text{mol}\cdot\text{K}}$ ) | <i>Substance</i>                            | <i>State</i> | $\Delta H_f^\circ$<br>( $\frac{\text{kJ}}{\text{mol}}$ ) | $S^\circ$<br>( $\frac{\text{J}}{\text{mol}\cdot\text{K}}$ ) |
|-----------------------------------|--------------|--|---|---|--------------|--|---|
| Ag                                | s            | 0  | 42.6  | Cl <sub>2</sub>                             | g            | 0  | 223.0   |
| Ag <sup>+</sup>                   | aq           | 105.79   | 72.7  | Cl <sup>-</sup>                             | aq           | -167.080   | 56.5  |
| AgCl                              | s            | -127.01  | 96.2  | ClO <sub>4</sub> <sup>-</sup>               | aq           | -128.10  | 182.0   |
| AgBr                              | s            | -100.4   | 107.1   | Cr  | s            | 0  | 23.8  |
| AgNO <sub>3</sub>                 | s            | -124.4   | 140.9   | Cr <sub>2</sub> O <sub>3</sub>              | g            | -1139.7  | 81.2  |
| Al                                | s            | 0  | 28.3  | Cu  | s            | 0  | 33.2  |
| Al <sup>3+</sup>                  | aq           | -538.4   | -321.7  | Cu <sup>+</sup>                             | aq           | +71.7  | 40.6  |
| AlCl <sub>3</sub>                 | s            | -704   | 110.7   | Cu <sup>+2</sup>                            | aq           | +64.8  | -99.6   |
| Al <sub>2</sub> O <sub>3</sub>    | s            | -1675.7  | 50.9  | CuO   | s            | -157.3   | 42.6  |
| Ba                                | s            | 0  | 62.8  | Cu <sub>2</sub> O                           | s            | -168.6   | 93.1  |
| BaCl <sub>2</sub>                 | s            | -858.6   | 123.7   | CuS   | s            | -53.1  | 66.5  |
| BaCO <sub>3</sub>                 | s            | -1216.3  | 112.1   | Cu <sub>2</sub> S                           | s            | -79.5  | 120.9   |
| Ba(NO <sub>3</sub> ) <sub>2</sub> | s            | -992   | 214   | CuSO <sub>4</sub>                           | s            | -771.4   | 107.6   |
| BaO                               | s            | -553.5   | 70.4  | F <sup>-</sup>                              | aq           | -335.35  | -13.8   |
| Ba(OH) <sub>2</sub>               | s            | -998.2   | 112   | F <sub>2</sub>                              | g            | 0  | 202.7   |
| BaSO <sub>4</sub>                 | s            | -1473.2  | 132.2   | Fe  | s            | 0  | 27.3  |
| Br <sub>2</sub>                   | l            | 0  | 152.2   | Fe(OH) <sub>3</sub>                         | s            | -823.0   | 106.7   |
| C                                 | s            | 0  | 5.7   | Fe <sub>2</sub> O <sub>3</sub>              | s            | -824.2   | 87.4  |
| CCl <sub>4</sub>                  | l            | -135.4   | 216.4   | Fe <sub>3</sub> O <sub>4</sub>              | s            | -1118.4  | 146.4   |
| CHCl <sub>3</sub>                 | l            | -134.5   | 201.7   | H <sub>2</sub>                              | g            | 0  | 130.6   |
| CH <sub>4</sub>                   | g            | -74.8  | 186.2   | H <sup>+</sup>                              | aq           | 0  | 0.0*  |
| C <sub>2</sub> H <sub>2</sub>     | g            | +226.7   | 200.8   | HBr   | g            | -36.29   | 198.6   |
| C <sub>2</sub> H <sub>4</sub>     | g            | +52.3  | 219.5   | HCO <sub>3</sub> <sup>-</sup>               | aq           | -689.93  | 91.2  |
| C <sub>2</sub> H <sub>6</sub>     | g            | -84.7  | 229.5   | HCl   | g            | -92.31   | 186.8   |
| C <sub>3</sub> H <sub>8</sub>     | g            | -103.8   | 269.9   | HF  | g            | -273.30  | 173.7   |
| CH <sub>3</sub> OH                | l            | -238.7   | 126.8   | HI  | g            | 26.50  | 206.5   |
| C <sub>2</sub> H <sub>5</sub> OH  | l            | -277.7   | 160.7   | HNO <sub>3</sub>                            | l            | -174.1   | 155.6   |
| CO                                | g            | -110.53  | 197.6   | HPO <sub>4</sub> <sup>-2</sup>              | aq           | -1299.0  | -33.5   |
| CO <sub>2</sub>                   | g            | -393.51  | 213.6   | HSO <sub>4</sub> <sup>-</sup>               | aq           | -886.9   | 131.8   |
| CO <sub>3</sub> <sup>-2</sup>     | aq           | -675.23  | -56.9   | H <sub>2</sub> O                            | l            | -285.830   | 69.9  |
| Ca                                | s            | 0  | 41.4  | H <sub>2</sub> O                            | g            | -241.826   | 188.7   |
| Ca <sup>+2</sup>                  | aq           | -543.0   | -53.1   | H <sub>2</sub> PO <sub>4</sub> <sup>-</sup> | aq           | -1302.6  | 90.4  |
| CaCl <sub>2</sub>                 | s            | -795.8   | 104.6   | H <sub>2</sub> S                            | g            | -20.6  | 205.7   |
| CaCO <sub>3</sub>                 | s            | -1206.9  | 92.9  | Hg  | l            | 0  | 76.0  |
| CaO                               | s            | -634.92  | 39.8  | Hg <sup>+2</sup>                            | aq           | 170.21   | -32.2   |
| Ca(OH) <sub>2</sub>               | s            | -986.1   | 83.4  | HgO   | cr,red       | -90.79   | 70.3  |
| CaSO <sub>4</sub>                 | s            | -1434.1  | 106.7   |   |              |  |   |
| Cd                                | s            | 0  | 51.8  |   |              |  |   |
| Cd <sup>+2</sup>                  | aq           | -75.92   | -73.2   |   |              |  |   |
| CdCl <sub>2</sub>                 | s            | -391.5   | 115.3   |   |              |  |   |
| CdO                               | s            | -258.35  | 54.8  |   |              |  |   |

\*The standard entropy of the H<sup>+</sup>(aq) ion is defined to be 0.

| Substance                       | State | $\Delta H_f^\circ$<br>( $\frac{\text{kJ}}{\text{mol}}$ ) | $S^\circ$<br>( $\frac{\text{J}}{\text{mol}\cdot\text{K}}$ ) |
|---------------------------------|-------|--|---|
| I <sup>-</sup>                  | aq    | -56.78   | 111.3   |
| I <sub>2</sub>                  | s     | 0  | 116.1   |
| K                               | s     | 0  | 64.2  |
| K <sup>+</sup>                  | aq    | -252.14  | 102.5   |
| KBr                             | s     | -393.8   | 95.9  |
| KCl                             | s     | -436.7   | 82.6  |
| KClO <sub>3</sub>               | s     | -397.7   | 143.1   |
| KClO <sub>4</sub>               | s     | -432.8   | 151.0   |
| KNO <sub>3</sub>                | s     | -494.6   | 133.0   |
| Mg                              | s     | 0  | 32.7  |
| Mg <sup>+2</sup>                | aq    | -467.0   | -138.1  |
| MgCl <sub>2</sub>               | s     | -641.3   | 89.6  |
| MgCO <sub>3</sub>               | s     | -1095.8  | 65.7  |
| MgO                             | s     | -601.60  | 26.9  |
| Mg(OH) <sub>2</sub>             | s     | -924.5   | 63.2  |
| MgSO <sub>4</sub>               | s     | -1284.9  | 91.6  |
| Mn                              | s     | 0  | 32.0  |
| Mn <sup>+2</sup>                | aq    | -220.8   | -73.6   |
| MnO                             | s     | -385.2   | 59.7  |
| MnO <sub>2</sub>                | s     | -520.0   | 53.0  |
| N <sub>2</sub>                  | g     | 0  | 191.5   |
| NH <sub>3</sub>                 | g     | -45.94   | 192.3   |
| NH <sub>4</sub> <sup>+</sup>    | aq    | -133.26  | 113.4   |
| NO <sub>2</sub> <sup>-</sup>    | aq    | -104.6   | 123.0   |
| NO <sub>3</sub> <sup>-</sup>    | aq    | -206.85  | 146.4   |
| N <sub>2</sub> H <sub>4</sub>   | l     | +50.6  | 121.2   |
| NH <sub>4</sub> Cl              | s     | -314.4   | 94.6  |
| NH <sub>4</sub> NO <sub>3</sub> | s     | -365.6   | 151.1   |
| NO                              | g     | +90.2  | 210.7   |
| NO <sub>2</sub>                 | g     | +33.2  | 240.0   |
| N <sub>2</sub> O <sub>4</sub>   | g     | +9.2   | 304.2   |
| Na                              | s     | 0  | 51.2  |
| Na <sup>+</sup>                 | aq    | -240.34  | 59.0  |
| NaCl                            | s     | -411.2   | 72.1  |
| NaF                             | s     | -573.6   | 51.5  |
| NaOH                            | s     | 425.6  | 64.5  |

| Substance                     | State | $\Delta H_f^\circ$<br>( $\frac{\text{kJ}}{\text{mol}}$ ) | $S^\circ$<br>( $\frac{\text{J}}{\text{mol}\cdot\text{K}}$ ) |
|-------------------------------|-------|--|---|
| Ni                            | s     | 0  | 29.9  |
| NiO                           | s     | -239.7   | 38.0  |
| OH <sup>-</sup>               | aq    | -230.015   | -10.8   |
| O <sub>2</sub>                | g     | 0  | 205.0   |
| P <sub>4</sub>                | s     | 0  | 164.4   |
| PCl <sub>3</sub>              | g     | -287.0   | 311.7   |
| PCl <sub>5</sub>              | g     | -374.9   | 364.5   |
| PO <sub>4</sub> <sup>-3</sup> | aq    | -1277.4  | -222  |
| Pb                            | s     | 0  | 64.8  |
| Pb <sup>+2</sup>              | aq    | 0.92   | 10.5  |
| PbBr <sub>2</sub>             | s     | -278.7   | 161.5   |
| PbCl <sub>2</sub>             | s     | -359.4   | 136.0   |
| PbO                           | s     | -219.0   | 66.5  |
| PbO <sub>2</sub>              | s     | -277.4   | 68.6  |
| S                             | s     | 0  | 31.8  |
| SO <sub>2</sub>               | g     | -296.81  | 248.1   |
| SO <sub>3</sub>               | g     | -395.7   | 256.7   |
| SO <sub>4</sub> <sup>-2</sup> | aq    | -909.34  | 20.1  |
| S <sub>2</sub> <sup>-</sup>   | aq    | +33.1  | -14.6   |
| Si                            | s     | 0  | 18.8  |
| SiO <sub>2</sub>              | s     | -910.7   | 41.8  |
| Sn                            | s     | 0  | 51.6  |
| Sn <sup>+2</sup>              | aq    | -8.9   | -17.4   |
| SnO <sub>2</sub>              | s     | -577.63  | 52.3  |
| Zn                            | s     | 0  | 41.6  |
| Zn <sup>+2</sup>              | aq    | -153.39  | -112.1  |
| ZnI <sub>2</sub>              | s     | -208.0   | 161.1   |
| ZnO                           | s     | -350.46  | 43.6  |
| ZnS                           | s     | -206.0   | 57.7  |